A HEAVY REACTION PRODUCT SPECTROMETER

A thesis submitted to the Department of
Physics of the University of Manitoba
in conformity with the requirements
for the degree of Master of Science

by

Peter McKenzie French

April 1967

ABSTRACT

Apparatus was designed and built to study heavy reaction particles from (p,x) reactions where x is a particle heavier than an alpha particle. The apparatus consisted of a ΔE-E counter telescope utilizing a proportional counter as the energy loss detector and a solid state counter for the total energy. The telescope had an energy threshold of 5 MeV for He^4, 7 MeV for He^6 and 11 MeV for Li^6 particles. An electrostatic separator was used to reduce the proton background entering the detectors.

The performance of the apparatus was checked with alpha particles from a $C^{12}(p,He^4)B^9$ reaction and appeared to be satisfactory. A preliminary search for (p,Li^6) reactions from C^{12} and F^{19} targets yielded negative results. Maximum differential cross sections of 0.5 μbarns/steradian were assigned for both targets.

ACKNOWLEDGEMENTS

The writer wishes to express his thanks to Dr. K.G. Standing for his constant encouragement and valuable advice during the construction and testing of the equipment and during the writing of this thesis, to E. Senicki for his help in the design and construction of the apparatus, and to J.J. Burgerjon, P. Bonsor and the cyclotron operating staff for the many hours of machine time. Thanks are also due to R. Batten, P. Lindsay, and other members of the workshop, and to F. Konopasek and his electronics staff for their helpful advice during the building of the equipment. The writer also owes a special debt of gratitude to his wife for her constant encouragement and for the typing of this thesis.

In a project of this type numerous other people were involved to whom the writer gives his thanks.

Finally, the writer wishes to express his indebtedness to the National Research Council for the research grants which made this work possible.

TABLE OF CONTENTS

TABLE OF CONTENTS (CONT'D)

LIST OF FIGURES

SECTION I

CHAPTER 1 INTRODUCTION

Considerable interest has arisen recently in the study of many-particle transfer reactions. These are reactions where a transfer of more than 3 particles occurs between the incoming particle and target nucleus. Once the reaction mechanism is well understood, such reactions should be of great usefulness in investigations of the structure of nuclei and in particular, should help in the qualitative study of nuclear "clustering".

Nuclear clustering is not a new idea. It has been known for some time that certain nuclei such as C^{12} are best described by an alpha particle model[1]. In addition, light nuclei shell model wave functions can be rewritten in cluster form, these clusters being groups of nucleons having the correct symmetry properties (angular momentum etc.) but otherwise not necessarily resembling the free nuclei[2]. Li^{6} may be viewed as an alpha plus deuteron and Li^{7} as an alpha cluster plus triton cluster, for example.

If this clustering really occurs in nuclei, then the transfer of such clusters in nuclear reactions should be greatly enhanced over the exchange of the same number of uncorrelated nucleons. Information could be gained about the structure of parent or daughter nuclei which would enable comparison with theoretically predicted wave functions[3].

The reaction mechanism may be direct or through the formation of compound states and experimental investigations are necessary to determine which predominates.

Deuteron induced many-particle transfer reactions have been performed recently with cross sections higher than might be expected considering they involve the transfer of 4 or more nucleons, and Coulomb barriers are high. In many cases the cross sections are comparable with or higher than the corresponding (p,He^4) cross sections.

Daehnick[3] and Gemmel[4,5] observed (d,Li^6), (d,Li^7) and (d,Be^9) reactions in C^{12} and F^{19} ($E_d \sim$ 12 to 15 MeV) and found that all reactions showed similar angular distributions. They were forward peaked and oscillatory in shape, with minima which were fairly regularly spaced (40^o - 50^o apart) and which moved closer together and to smaller angles with increasing atomic weight. This suggested a direct reaction mechanism and DWBA fits to the experimental differential cross sections showed qualitative agreement. The theoretical minima were deeper than those found experimentally, possibly because of a noticeable compound nuclear contribution.

Slee[6] has done similar (d,Li^6) work at deuteron energies of about 21 MeV on F^{19} targets and observed comparable yields.

Not much has been done on proton induced many-particle transfer reactions. Lindsay[7] quotes some 35 to 55 MeV work done by Furukawa[8] on the reaction $Al^{27}(p,Be^7)Ne^{21}$ and

postulates a compound nuclear effect. The reaction $Mg^{24}(He^4,Be^7)Ne^{21}$ proceeds through the same compound nucleus but Lindsay found a cross section some 4 times higher than Furukawa's. He interprets this breakdown of the hypothesis of independent formation and decay of the compound nucleus on the basis of angular-momentum limitations on the particle emission probabilities.

Heikkinen[9] has observed the inverse reactions $C^{12}(Li^6,p)O^{17}$ and $C^{12}(Li^6,d)O^{16}$ at incident Li^6 energies between 4.5 and 5.5 MeV. He postulates a direct reaction mechanism with a significant compound nuclear contribution for certain states of the residual nuclei.

The conclusions these authors have reached indicate that the reaction mechanism is not simple. The high probability for He^4 or Li^6 pickup in Daehnick's results indicate alpha and deuteron clustering in nuclei and a direct reaction mechanism. The work of Lindsay and of Furukawa, however, indicates that He^5 clustering is less probable and reactions thought to proceed by direct He^5 pickup might be better characterized by a compound nuclear process, showing energy resonances. Other effects such as shell closure and angular momentum transfer must also be considered.

Certain experimental difficulties limited the range of reaction particles that could be observed with 50 MeV protons at the University of Manitoba. The cross sections are small and Q values very negative for these reactions,and as the

particle mass and charge increase, its range diminishes rapidly and its unique identification is difficult. Also Coulomb barrier effects become appreciable. A magnetic analyzer was not available and thus a counter telescope (ΔE-E) system was employed and the particle range in the counters became an important factor. Proton induced reactions of the type (p,x) are most convenient experimentally if the reaction product x is stable or relatively long lived. This fact, together with the previous considerations, limited x to He^6, He^8, Li^6, Li^7, Li^8, or Li^9.

SECTION II THE APPARATUS

CHAPTER 2 SOLID STATE DETECTOR

Counter System

In any proton induced reaction, the reaction product of interest is always accompanied by a number of other particles and one of the tasks an experimenter is faced with is the identification of these interesting particles. Various techniques have been used, but one of the simplest methods is an E,dE/dx counter telescope system and we decided to employ it.

A counter telescope consists of a thin transmission counter followed by a thicker total energy detector. The thin counter measures the rate of energy loss dE/dx while the thicker counter stops the particle and measures its total energy, E (actually $E-(dE/dx)\Delta x$). E and dE/dx are related through Bethe's energy loss formula

$$-\frac{dE}{dx} = \frac{2\pi e^4 Mz^2}{mE} NZ \ln\frac{4mE}{MI}$$

where m is the electronic mass, ze is the charge of the particle of mass M and N is the atomic density, Z the atomic number and I the average atomic excitation potential of the stopping material.[10]

The obvious choice was solid state detectors because of their excellent resolution, reasonably fast response, compactness and ease of operation. It will be shown, however, that thickness considerations limited their usefulness for the

thin counter.

Figure 1 shows the range-energy relationship for various reaction products as determined from energy loss calculations by Williamson and Boujot[11]. The energy loss for thin absorbers may be found by subtracting out the absorber thickness at the incident particle energy or more exactly from stopping power calculations based on Williamson's and Boujot's work. This figure clearly shows that the transmission counter should be at most 25 to 30 microns thick so that heavier particles of about 10 to 20 MeV can be passed. At the time these counters were being considered, however, no solid state detectors with reasonable uniformity seemed to be available at these thicknesses. It was decided therefore, that only the total energy counter would be a solid state counter.

The counter purchased was a lithium drifted, silicon detector* with 0.5 mm depletion depth and 200 mm^2 surface area. The large surface area was chosen to increase counting rates - the scattering chamber available was a 40 inch diameter tank and the cross sections for heavy particle reactions were thought to be quite low. The 0.5 mm thickness was sufficient to stop 33 MeV alphas and heavier particles of higher energy. Calculations of various reactions indicated that these heavier particles would have energies less than about 35 MeV and thus the detector was quite adequate. An added advantage was that the counter was relatively thin for protons and deuterons. For example, protons between 20 and 50 MeV

* Simtec Ltd.,3400 Metropolitan Blvd. East, Montreal.

FIGURE 1

PARTICLE RANGES IN SILICON

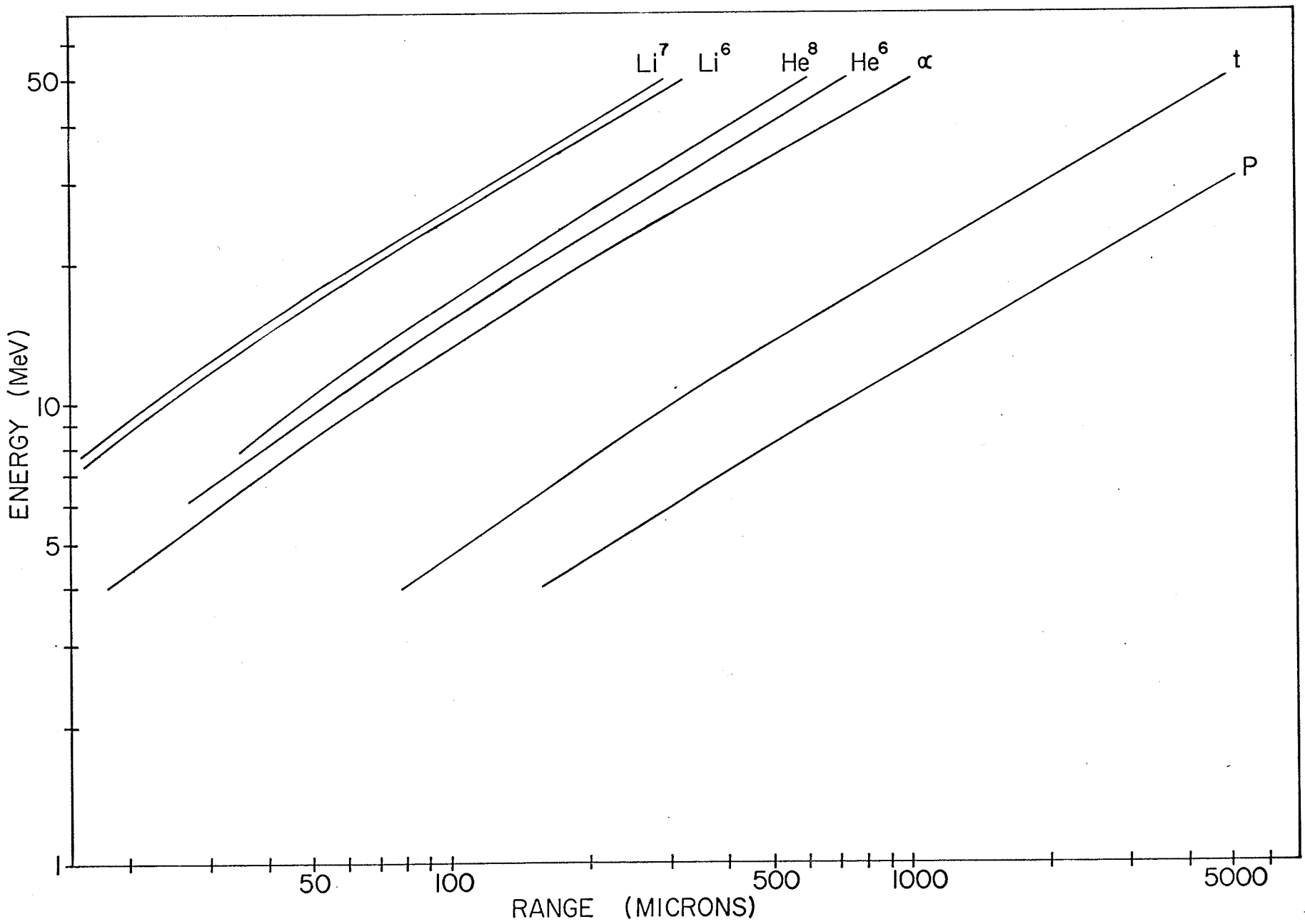
Li7
Li6
He8
He6
α
t
P
50
10
5
1
ENERGY (MeV)
50
100
500
1000
5000
RANGE (MICRONS)

would lose between 3 and 1 MeV, while deuterons in the same energy range would lose between 5 and 2 MeV. This would aid in the discrimination between lighter and heavier particles.

The detector was mounted in a thick brass holder to shield it from stray radiation. Later on, the holder was modified by reducing the aperture from 16 mm to 8.4 mm diameter to eliminate suspected nonuniformity of the active area.

Detector Characteristics

Preliminary tests were done to determine the detector characteristics and the results were quite satisfactory. The linearity was checked with alpha particles of three energies - 5.48 MeV from Am^{241} and 6.05 and 8.78 MeV from a Th source* - and was within 0.1%. No dead layer correction was made, and the linearity of the detector indicated that it was quite small - the manufacturer specified a 0.2 micron window.

The resolution was tested at 25°C and at about -25°C with a thermoelectric cooler when the counter was first received. The cooled run yielded FWHM values of 68 keV, 79 keV, and 45 keV for the alpha energies 5.48, 6.05 and 8.78 MeV respectively, while the uncooled run yielded 79 keV, 90 keV, and 68 keV, for the same energies. The 5.48 and 6.05 MeV alphas have multiple energy structure, while the 8.78 MeV has just one peak and this accounts for the lower width for the higher energy particle.

* 6.05 MeV from Bi^{212} and 8.78 MeV from Po^{212}

The manufacturer specified a FWHM value of 45 keV (cooled) for the 5.48 MeV alpha and the higher values we observed could be due to increased electronic noise, or the worsening of resolution with time. The "age" of the counter seemed to play an important part in its operation. The dead layer and resolution worsened with time even when the counter was not exposed to radiation.

The resolution changed with bias voltage, as expected, and yielded a minimum at 55 volts, but the tests were done at 70 volts since this was considered a reasonable operating bias to facilitate charge collection from more energetic particles. In any case, the FWHM value at 70 volts was within 8 keV of that at 55 volts and the cyclotron proton energy spread was known to be at least 300 keV.

All silicon solid state counters are susceptible to radiation damage, and the effects of the damage were quite evident in this counter. The resolution steadily worsened with running time as the detector was used to measure charged particle reaction energies. Charge collection efficiencies for higher energy alphas seemed to decrease and the counter bias had to be raised to 110 volts before reasonable spectra were observed. This was presumably caused by an increase in trapping centers as the radiation damage increased. In addition the bias level then had very little effect on resolution.

The dead layer also increased, but this effect

seemed to depend on the method of biasing. When the detector was first used in the tests described above, the dead layer was very small, but after a period of two months unbiased, the dead layer increased to 3.1 microns and this had to be taken into account for energy calibrations. No increase in dead layer was observed while the counter was continuously biased, but after a short unbiased period near the end of the runs, the thickness increased to 5 microns. Two alpha source energies were used to experimentally determine the dead layer.

The FWHM values for natural alphas doubled over a 2.5 month period and values of 150 to 200 keV were typical at the end of the experimental program. This worsening of the resolution was not well understood, but it was concluded that it was an inherent detector property and not due to noise pickup or higher temperatures in the cyclotron experimental area - removing the detector from this area had no effect on its performance. The large dead layer, counter "age", or charge collection efficiencies may have been factors.

Attempts were made to improve the resolution, as recommended by the manufacturer. The counter was left at maximum recommended bias for several days and then left unbiased for several days. No improvement in resolution was seen, however.

Associated Electronics

The electronic systems are shown in figure 12. The detector was biased with a Tennelec Model 901 RM 0 to 200 volt unit. A tube type 100-B preamplifier was used and was found quite satisfactory. Other workers in the lab had found that solid state preamplifiers were subject to excessive pickup when the external beam was on. All preliminary tests utilized a two dimensional analyzer* in the 1024 channel single parameter mode. The data was punched on paper tape and the tape was fed to a tape to typewriter converter to obtain a typed output.

* ND Series 160, Nuclear Data Inc., P.O. 451, Palating, Illinois.

CHAPTER 3 THE PROPORTIONAL COUNTER

Energy Loss Counter

A solid state detector would seem the best choice for the dE/dx counter, but as mentioned in Chapter 2, we were unable to obtain one sufficiently thin and uniform enough to be of use with heavy reaction particles. This left gas counters as the alternative, since the gas pressure and counter diameter could be set at some optimum value for a reasonable particle energy loss.

Of the two types of gas counters which were suitable, a proportional counter seemed better than a pulse ionization chamber. Besides being easier to construct and operate, a proportional counter is more robust and gives an output pulse some hundreds or thousands of times as great as an ionization chamber.

Theory

A proportional counter is a gas filled device with two electrodes between which is applied a potential difference. It is similar to an ionization chamber, in that particles are detected by means of the ionization they produce in the gas but a proportional counter utilizes gas multiplication. It produces an output pulse many times larger than would be obtained from an ionization chamber for the same initial ionization. This gas multiplication results when the electric

field in some part of the active volume of the counter is sufficiently high to cause the primary ionization electrons to produce secondary ionization - the free electrons gain enough energy between molecular collisions to cause additional ionization.

The counter is strictly proportional over a limited range of applied potential since the multiplication process must be such that interactions between avalanches produced by individual primary electrons must be small. If this is the case, and if each initial ion pair results in the production of a specific average number of collected ion pairs, then the output signal is proportional to the initial ionization. Then if a definite amount of energy is required to produce each initial ion pair, independent of the energy of the ionizing particle, the output pulse is proportional to the energy lost by this particle. The proportional counter is thus energy sensitive.

For a cylindrical proportional counter, the field is intense enough to produce gas multiplication only in the immediate neighborhood of the central wire (anode) and thus most of the secondary ionization is produced here. These secondary electrons traverse only a small fraction of the total applied voltage and so contribute very little to the output pulse. It follows, therefore, that the major portion of this output is produced by the motion away from the wire of the positive ions. These ions induce a charge on the wire and as they drift toward the cathode, the change in induced

charge at the wire causes the output pulse. These ions fall through most of the voltage drop while moving in the high field region near the wire so that despite their low mobility, the signal rise is not slow.

The theory and characteristics of proportional counter operation will be reviewed briefly. Excellent detailed accounts are available in the literature.[12,13,14]

Early investigations showed that the average energy required to produce an ion pair in a proportional counter gas was surprisingly constant with the energy and not very different for different particles.[15] This was especially true of hydrogen and the noble gases, and has led to widespread use of argon in proportional counters where accurate energy determination is required. Jesse[16] has shown that alpha particle energy loss and resulting ionization are proportional to each other within 0.5% in argon.

Within about 10^{-7} sec after the passage of the ionizing particle through the gas, the free ionization electrons will be reduced in energy to a few electron volts and will begin to drift toward the center wire with a velocity that depends on the local electric field, the gas pressure, and the gas composition. When near enough to the center wire, these electrons will have gained sufficient energy to produce an avalanche and the motion of the resulting positive ions will produce the output pulse. It becomes quite important, therefore, to ensure that the initial electrons are

not lost by recombination if the output pulse is to be proportional to the energy lost in the counter by the ionizing particle.

Wilkinson[12] has shown that there is no appreciable recombination in proportional counters provided there are no electronegative impurities present. The counter operation is severely hampered if O_2, H_2O, NH_3, HCl, SiF_4 or halogens contaminate the gas, and every precaution should be taken to exclude their presence.

As already mentioned, it is the positive ion motion away from the anode which results in the output pulse for a cylindrical counter. Most of these ions are produced close to the center wire and an important property results - the pulse size is independent of the position of the track within the counter and its shape is the same for all pulses. This pulse shape has been calculated by Wilkinson.[12] If K is the ionic mobility in the gas, then the voltage pulse shape P(t) is given by

$$P(t) = -\frac{e}{C}\,\frac{\ln\left[\left(\frac{2VKt}{a^2 \ln(b/a)}\right) + 1\right]}{2 \ln(b/a)} \qquad 3.1$$

and the pulse is collected after a time

$$t = \frac{(b^2 - a^2) \ln(b/a)}{2VK} \qquad 3.2$$

at which time $P(t) = -(e/C)$.

The wire radius is a, the counter radius b, the applied

voltage is V, and the counter capacitance is C.

Although the charge collection time is quite long (typically hundreds of microseconds) the initial rise is very rapid and by proper counter construction half the maximum pulse height may be realized in less than 1 μsec. This rapid initial rise means that short clipping times may be used, thus making the pulses very short without much loss of pulse height. Wilkinson[12] showed that the R-C clipped pulse shape $v(\tau)$ is given by

$$v(\tau) = \frac{1}{2 \ln(b/a)} \frac{1}{S} \frac{1}{\tau + (a^2/b^2)} \qquad 3.3$$

where τ is a convenient time unit related to the actual time t by

$$\tau = \frac{2VK}{b^2 \ln(b/a)} t \, . \qquad 3.4$$

S is defined in units of τ^{-1} by S = (1/RC), where RC is the clipping time constant in τ units.

The time at which $v(\tau)$ is a maximum is given by

$$1/S\tau_{max} = \ln(b^2/a^2) \, \tau_{max} \qquad 3.5$$

provided the differentiation is strong ($1 \ll S \ll b^2/a^2$). The pulse drops to half maximum after a time

$$\tau_{\frac{1}{2} max} = \frac{2}{\left[S \ln(b^2/a^2)\right]^{0.5}} + \frac{a^2}{b^2} \, . \qquad 3.6$$

The fact that P(t) remains the same for all pulses means that the counter remains accurately proportional even under sharp differentiation and thus fast counting is possible.

Another effect which influences the counting speed is the electron mobility. Wilkinson[12] shows that an electron produced at a distance x_o from the centre of the chamber is collected after a time

$$t = \frac{x_o^{1.5} - a^{1.5}}{1.5K_{e-}\left[\frac{V}{\ln(b/a)}\right]^{0.5}} \quad . \qquad 3.7$$

K_{e-} is the electron mobility and is given by

$K_{e-} = (1.6 \times 10^{-6})(E^{0.5}/P)$ where E is the local electric field (V/cm) and P the gas pressure in mm of Hg. The electron mobility is greatly increased if impurities are introduced to a pure gas. Bortner[17] has shown that electron drift velocities in a mixture of 90% argon and 10% methane are increased about 10 times over those in pure argon.

This introduction of a molecular gas impurity serves other useful purposes also. Metastable states of lifetime 10^{-4} sec or longer are formed chiefly in pure noble gases but the addition of small amounts of any molecular gas results in rapid de-excitation collisions and thus eliminates unwanted double pulsing effects.

It is worthwhile now, to summarize the precautions necessary to insure a multiplication value (A) which is con-

stant with time and doesn't depend on the position of the particle track.[12]

(1) The voltage supply must be well stabilized.

(2) A should be kept as small as possible.

(3) Some stabilizing gas should be added.

(4) No electronegative impurities should be present.

(5) The ionization should take place in regions of good wire geometry.

(6) The wire should be accurately circular and uniform and run accurately on the axis of the counter.

For multiplication greater than about 10, A is best given by

$$A = C_1 \exp[(V - V_p)/C_2]$$

where C_1 and C_2 are constants and V_p is the starting potential for proportional counter action. Thus an increase in V (usually 50 to 100 volts) doubles A.

In general, the resolution of a proportional counter is affected by the energy loss distribution for particles passing through the entrance window and the counter, fluctuations in the total ionization produced, statistical variations in the multiplication process, and electronic noise.

The theory for energy loss distributions has been

developed by Landau,[18] Symon,[19] and Seltzer and Berger,[20] and summarized by Rossi[21] and no attempt will be made here to outline it. Landau deals with thin absorbers only (energy loss less than 10% of initial energy) while Symon treats thick absorbers (energy loss greater than 10% of initial energy) as well as thin. Seltzer and Berger discuss the more rigorous treatment of Vavilov[22] which is also applicable to both thin and thick absorbers. Calculations of energy distributions are made later in this chapter and it suffices now to say that the widths of these distributions are usually greater than 10% of the energy loss.

Fano[23] has shown that if a definite amount of energy is lost in hydrogen, then the value of the mean square deviation in the number of ion pairs is between one-third and one-half of that expected if the process was governed by a Poisson distribution. If J_o is the mean number of ion pairs and J the actual number, then

$$\langle (J - J_o)^2 \rangle_{av} = FJ_o$$

where Fano suggests $F \cong 0.4$ for hydrogen, and assumes that F is of the same order of magnitude for other gases. If we assume $F \cong 1$ for argon, then if a definite amount of energy, typically 300 keV, is lost in the gas, the mean number of ions produced is about 10^4 and the root mean square deviation is about 10^2 or about 1.0% of the mean number of ions produced.

A theory of statistical fluctuations in the multi-

plication process has been developed by Snyder[24] and others and the results are presented here. If N electrons arrive at the wire corresponding to M initial electrons, and $\overline{N}$ and $\overline{M}$ are their respective mean values, then the relative mean square fluctuation in the total number of particles N arriving at the wire is given by

$$\frac{\overline{N^2} - \overline{N}^2}{\overline{N}^2} = \frac{\overline{M^2} - \overline{M}^2}{\overline{M}^2} + \frac{1}{\overline{M}} - \frac{1}{\overline{N}} \quad .$$

Now, $\overline{N}/\overline{M}$ is equal to the multiplication, and is quite large (100 to 1000) for proportional counters so the last term on the right side of the above equation may be neglected. If we assume a Poisson distribution, then

$$\frac{\overline{M^2} - \overline{M}^2}{\overline{M}^2} = \frac{1}{\overline{M}}$$

and thus

$$\frac{\overline{N^2} - \overline{N}^2}{\overline{N}^2} = \frac{2}{\overline{M}} \quad .$$

Thus the multiplication has the effect of doubling the relative variance in the original number of ions. The variance in the initial number of ions is just $\overline{M}$ and the root mean square deviation is $(\overline{M})^{0.5}$ and thus the variation in the number of electrons reaching the center wire is just $(2)^{0.5}$ that of the variation in the number of electrons initially produced. For the typical case mentioned above, the multiplication process introduces a root mean square deviation of about 1.4%.

The electronic noise is best determined experimentally by feeding equal artificial pulses through the system or by observing the noise level on an oscilloscope but generally it is no lower than 50 keV.

Design Restrictions

The primary consideration in designing the counter was to ensure that heavy reaction particles would not be stopped or lose too much energy in the counter gas itself or in the windows. Argon was chosen as the counter gas since the energy required to create one ion pair in argon is closely independent of the particle energy. Argon has the added advantage of a relatively low starting potential for proportional counter action. Mica was rejected in favor of mylar as a window material. Mylar is fairly robust and available in thickness down to 0.25 mg/cm^2, while it was found that mica thicknesses of less than 1 or 2 mg/cm^2 were difficult to obtain.

Figures 2 and 3 show the rate of energy loss in argon ($15^{o}C$ and 760 mm Hg) and mylar respectively, for various reaction products. The argon curves are calculated from proton energy loss tables by Aron[25], and the mylar curves are determined from stopping power calculations by Williamson and Boujot[11] for the constituent elements of mylar, $(C_5H_4O_2)_N$.

The proportional counter gas used was actually a mixture of 90% argon and 10% methane, but the effect of the

FIGURE 2

ENERGY LOSSES IN ARGON

(15°C and 760 mm Hg)

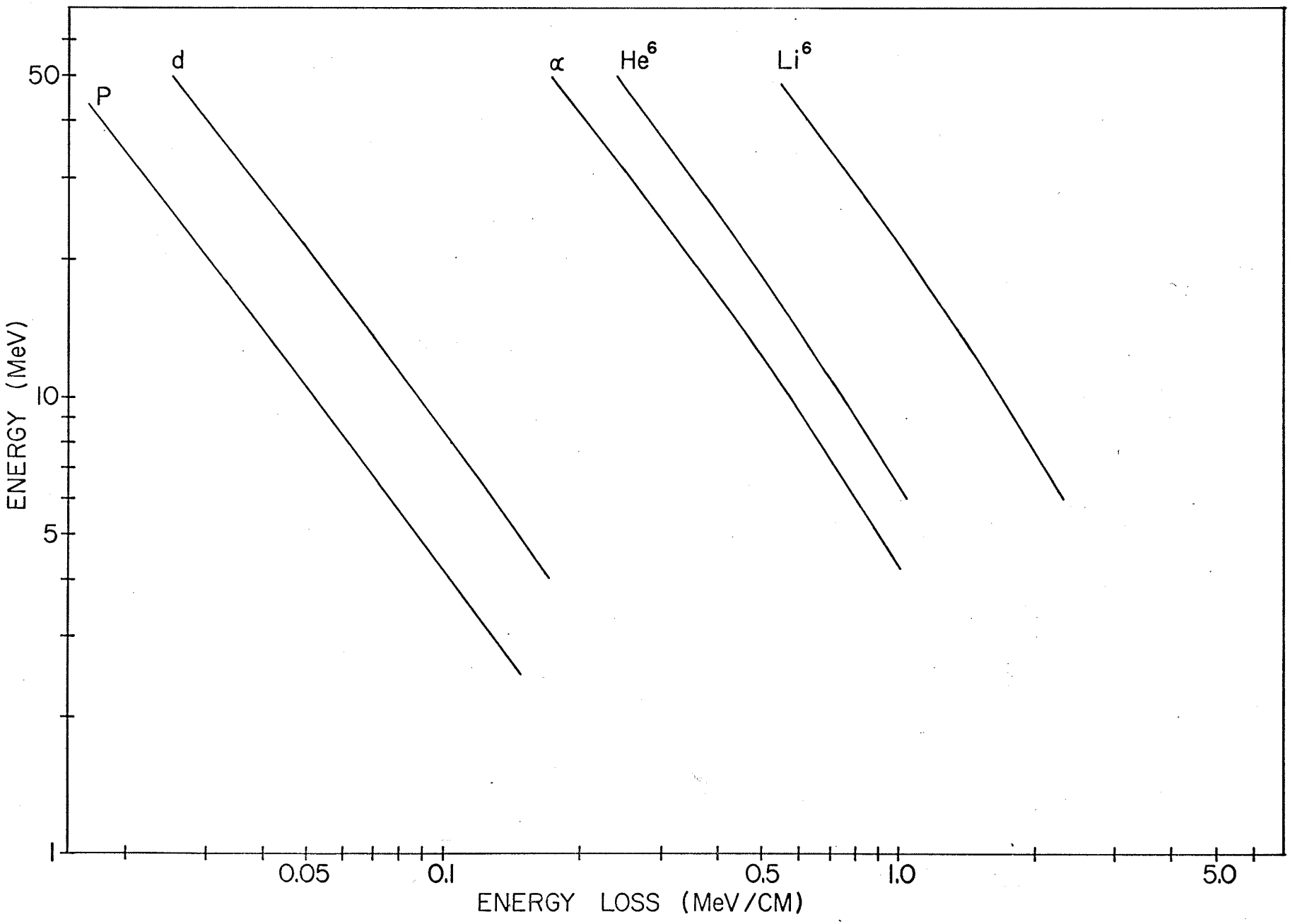
P
d
α
He6
Li6
50
10
5
1
ENERGY (MeV)
0.05
0.1
0.5
1.0
5.0
ENERGY LOSS (MeV/CM)

FIGURE 3

ENERGY LOSSES IN MYLAR

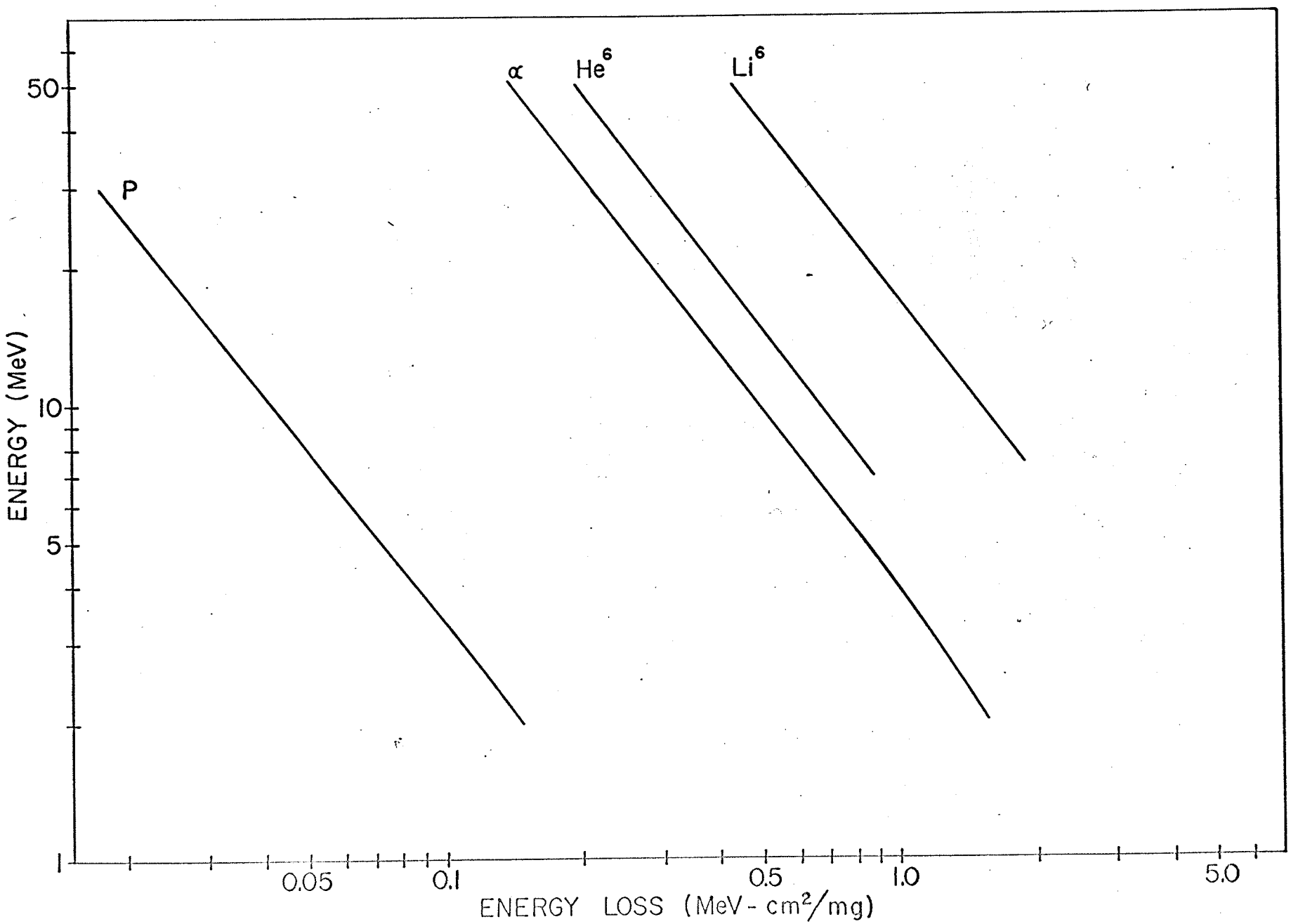
50
10
5
1
ENERGY (MeV)
P
α
He⁶
Li⁶
0.05
0.1
0.5
1.0
5.0
ENERGY LOSS (MeV - cm²/mg)

methane has been ignored in Figure 2. At the low energies (5 to 8 MeV) used to calibrate the proportional counter, the error in reading the graph was estimated to be about 5%, while the methane additive would change the energy loss by less than 1%.

The energy loss in the mylar windows can be made less than 1 MeV, even for Li^6 at 10 MeV, by a window thickness of about 0.25 mg/cm^2, and energy losses of only a few hundred keV are possible in a 1 inch diameter counter by varying the argon pressure.

Final Design

The proportional counter is shown in Figure 4. The casing was made of brass and measured 15.88 cm in length and 3.33 cm in diameter. The inside diameter was 2.66 cm and the gas filled region comprised 10.16 cm of the length. Gas inlet and outlet 0.64 cm O.D. brass pipes were situated 3.18 cm from each end of the counter and the counter was sealed vacuum tight with two brass plugs and two kovar seals along the axis of the counter.

The center wire was of tungsten (0.013 cm diameter) and was accurately centered along the counter axis by the kovar seals. Small hypodermic needles were slipped over the wire at each end of the counter to precisely define a "counting volume". The thickening of the wire would reduce the gas multiplication to a very low value at these points,

FIGURE 4

THE PROPORTIONAL COUNTER

A Terminal
B Gas Inlet
C Kovar Seal
D Hypodermic Needle
E Tungsten Wire
F Window

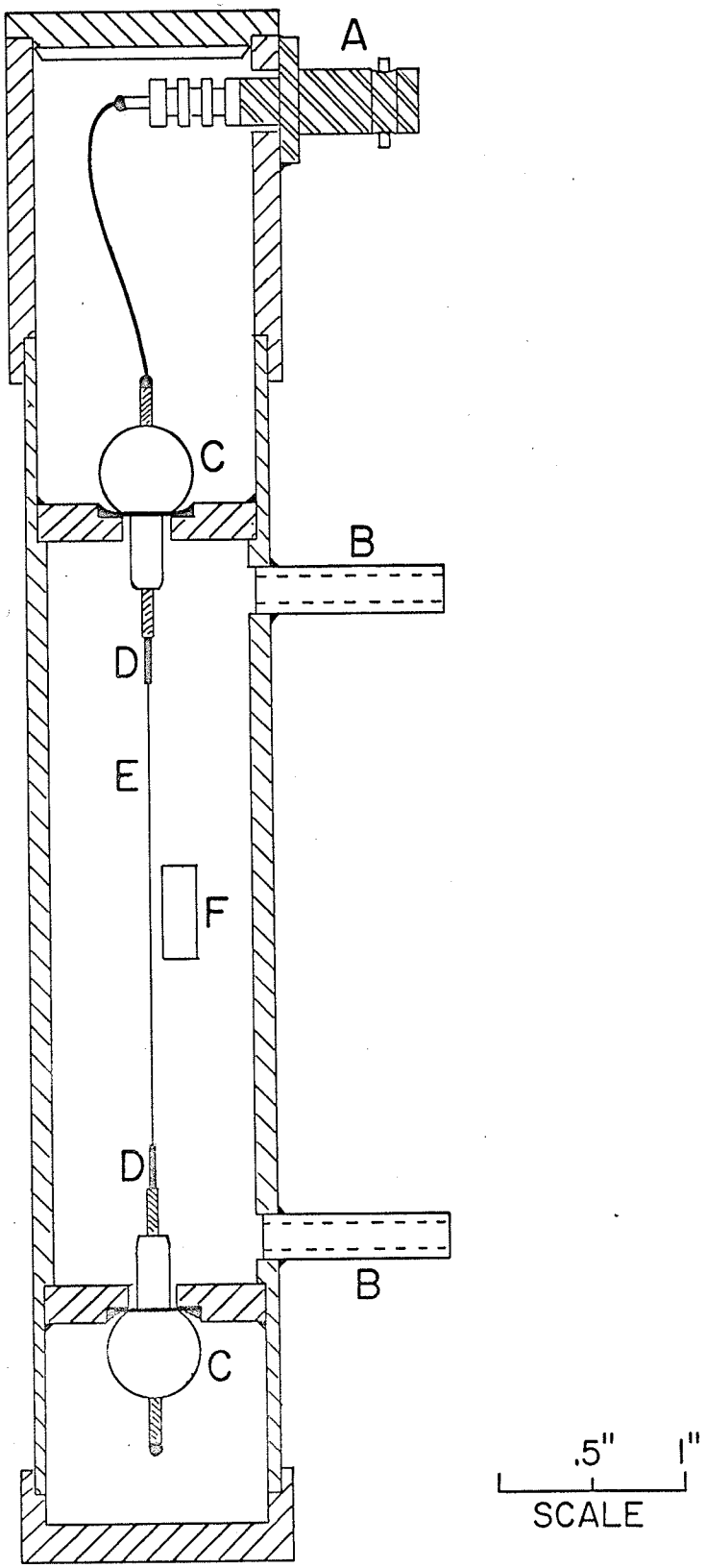
A
C
B
D
E
F
D
B
C
.5"
1"
SCALE

but should not distort the radial nature of the field significantly. The counting volume thus defined comprised 5.72 cm of the counter length so the ionization would take place in regions of good wire geometry.

The wire itself was examined under a microscope and was found to be quite accurately circular in cross section. The counter was thoroughly cleaned and immersed in dilute hydrochloric and nitric acid, followed by distilled water and acetone to remove all traces of solder flux and other contaminants.

Two windows were situated at the center of the counter, and were offset to prevent particles from striking the center wire. The windows measured 1.27 cm by 0.48 cm. The counter was machined flat at the window positions to ensure that the two windows would be parallel to each other and thus present a uniform path length through the gas filled region for particles passing through any part of the windows.

The windows were covered with mylar (1.23 mg/cm^2) and glued into place with a pressure cement.* Brass window frames were clamped over the mylar window to prevent slow leakage of the gas caused by the excess pressure on the inside of the counter working the mylar loose when the counter was in the evacuated scattering chamber.

A mixture of 90% argon and 10% methane was employed and a facility for varying the gas pressure in the counter was used. This was necessary since the windows could toler-

* Eastman-Kodak, # 910 Cement

ate only about one-half atmospheric pressure and gas pressures had to be equalized everytime the scattering chamber was vented. In addition, gas pressures could be set for optimum particle energy loss or optimum counter voltage. The counter pressure was set and maintained with a ballast tank and argon cylinder and regulator. The gas line was lead into the scattering chamber through a rotating bottom plate so that the counter could be set any angle with respect to the incident proton beam.

Some theoretical characteristics of counter operation were considered in arriving at the final design. The maximum time required to collect primary electrons was calculated from equation 3.7 for some typical counter parameters. V was taken as 1000 volts, 1.62 cm as the counter radius, and 0.5 atmospheres as the counter pressure. The result was 0.7 μsec for pure argon and less than 0.1 μsec for the argon-methane mixture. Thus if no electronegative impurities were present to contaminate the counter, the electron collection would be fairly rapid.

Equations 3.1 and 3.2 were used to find the undifferentiated pulse shape. The time required for the pulse to reach one-half maximum value was found to be

$$t_{\frac{1}{2}\ max} = 11 \times 10^{-6}\ (P/V)$$

while the whole pulse is collected after a time

$$t_{max} = 2.3 \times 10^{-3}\ (P/V)$$

where P is the gas pressure in mm of Hg (760 mm Hg = 1 atmosphere) and V is the applied voltage. For some typical proportional counter parameters, (V = 1000 volts and P = 0.25 atmospheres) it was found that $t_{\frac{1}{2}\ max} = 1.4\mu$ sec and $t_{max} = 290\mu$ sec - much greater than the electron collection time.

Some preliminary theoretical work indicated that reasonably good differentiation without much loss in pulse height would occur if an S value between 50 and 100 was used (equations 3.3 to 3.6). For S = 80, RC = 1.25×10^{-2} in τ units or a clipping time constant of 3.5μ sec. This clipped pulse was found theoretically to have a maximum at 9.4μ sec and dropped to one-half this maximum value 32.3μ sec later. The rise time was quite long compared to solid state counters, but was considered adequate for the intended purpose. The pulse length limited counting rates to about 10^4 per second but this was also considered quite adequate for the counting rates expected.

The theoretical resolution of the counter was determined by calculating particle energy spreads in the counter gas and entrance window for a gas pressure of 0.4 atmospheres and window thickness of 1.23 mg/cm^2. Two typical alpha energies were considered: 5.48 MeV from an Am^{241} source and 24 MeV from a (p,He^4) reaction.

The energy loss of the Am^{241} alpha was calculated to be 0.96 MeV in the entrance window (Figure 3), and 1.02 MeV

in the gas (Figure 2). Symon's[19] theory of energy-loss fluctuations was applied and the FWHM value of the energy loss distribution in the gas was 24% of the energy loss in the gas or about 250 keV.

The fluctuation in the number of primary ion pairs produced, and the statistical fluctuation in the multiplication process, amount to a spread of about 1.1% which is negligible compared to the fluctuation in energy loss.

The observed electronic noise was about 100 keV and this, combined with the energy spreads, was calculated to give a total resolution of about 26% for the 5.5 MeV alpha particles.

A similar calculation for 24 MeV reaction alpha particles yielded an energy loss of 324 keV, and energy spread 48% of this energy loss in the gas. Together with the electronic noise, the final energy spread is about 57% of the energy loss in the gas assuming perfect resolution in the beam from the target. Actually the beam had $\lesssim$ 3% spread, approximately, but this would not contribute significantly to the counter resolution.

The electronics associated with the proportional counter are shown in Figure 12. A well stabilized power supply was used to bias the counter and the signal was taken from the center wire. The high voltage was decoupled from the signal by the clipper circuit which had a time constant of 3.3 μsec. Owing to the low counter capacitance (about 1pF)

and high cable capacitance (about 25 pF per foot) the voltage preamplifier was placed as close to the counter as possible to avoid loss of pulse height. The preamplifier was a standard photomultiplier-preamplifier and had a gain of about 30. An oscilloscope was used to determine the proper counter operating voltage every time the argon gas was changed, and the pulse was monitored in the control room.

The pulses from the experimental area were fed into an RC amplifier and then to the Nuclear Data analyzer.

Counter Characteristics

The proportional counter operating characteristics were tested at a number of different pressures (Figure 5) with an Am^{241} alpha source. The pulse height was monitored right after the clipper circuit and plotted against applied voltage to determine the linear proportional region.

It was decided that the pressure best suited for the intended experiments was about 0.4 atmospheres. The operating region was quite linear here and the energy losses for heavy particles were reasonable (Figure 2). In addition, the gas multiplication was not too large in this region.

The resolution of the counter was tested with Am^{241} alpha particles at a gas pressure of 0.4 atmospheres and 1650 volts bias. The energy loss spectrum is shown in Figure 6. The measured resolution of 28% agrees fairly well with the theoretical resolution of 26% calculated above (p. 29).

FIGURE 5

PROPORTIONAL COUNTER CHARACTERISTICS AT VARIOUS GAS PRESSURES (Am^{241} Alpha Source)

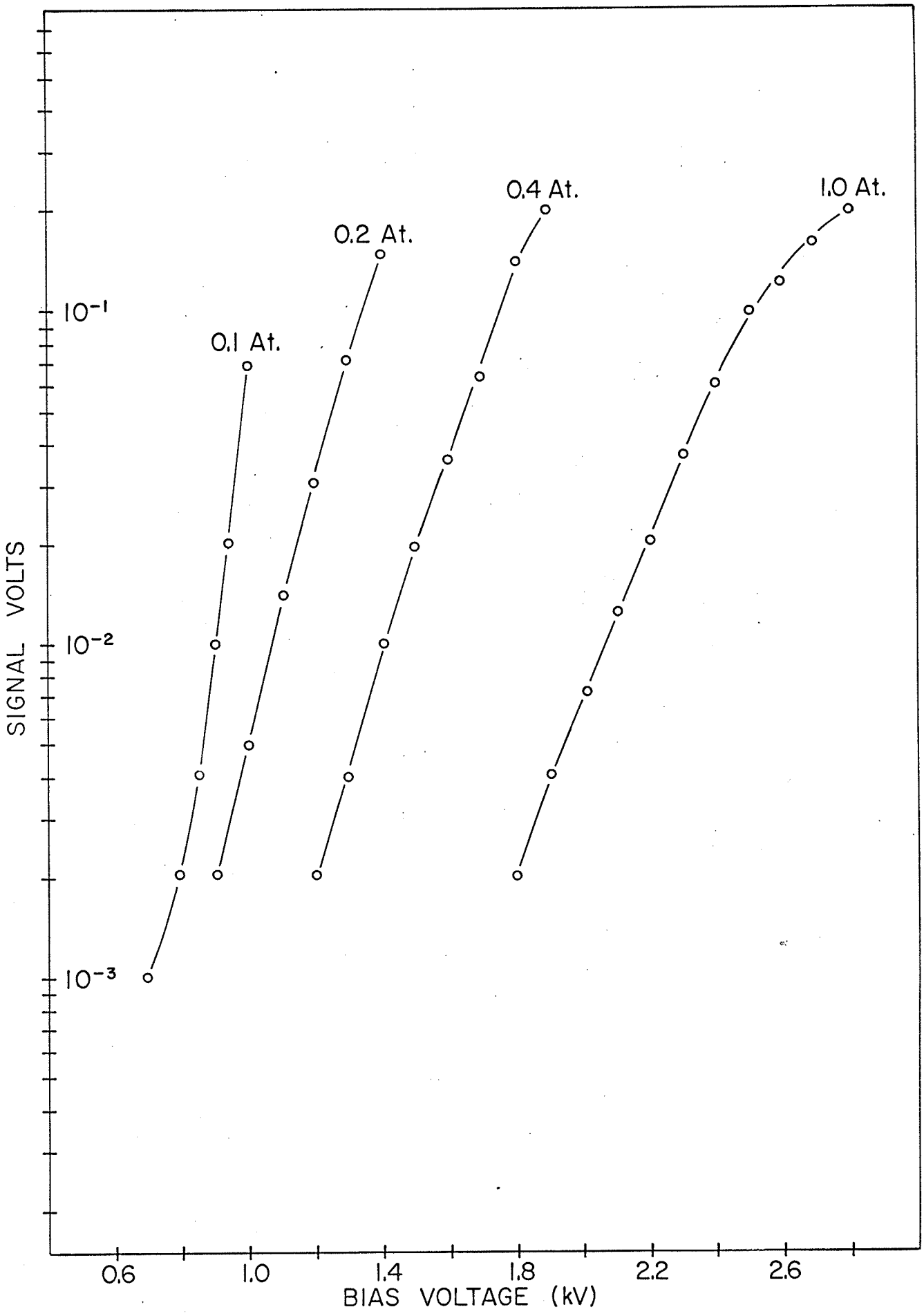
0.4 At.
1.0 At.
0.2 At.
0.1 At.
10^{-1}
10^{-2}
10^{-3}
SIGNAL VOLTS
0.6
1.0
1.4
1.8
2.2
2.6
BIAS VOLTAGE (kV)

FIGURE 6

PROPORTIONAL COUNTER RESOLUTION FOR

Am^{241} ALPHAS AT 5.48 MeV

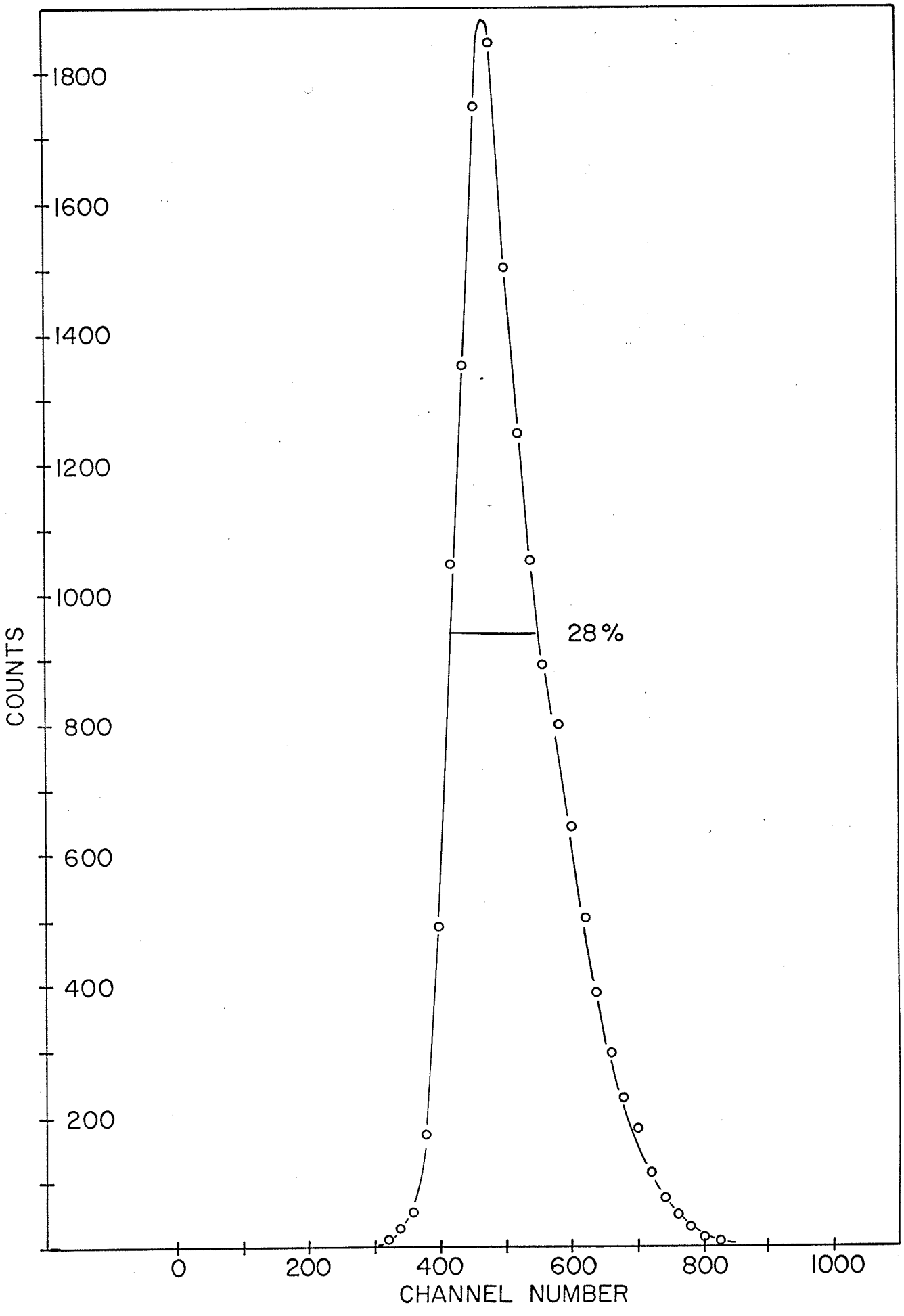
1800
1600
1400
1200
1000
800
600
400
200
COUNTS
28%
0
200
400
600
800
1000
CHANNEL NUMBER

The pulse lengths (about 20 μ sec) were typically shorter than calculated theoretically (p.28) owing to the capacitor coupled input to the preamplifier reducing the effective differentiating capacity.[12]

CHAPTER 4 THE ELECTROSTATIC SEPARATOR

Separator Theory

Elastic and inelastic protons normally form the bulk of the background in any proton induced reaction, particularly at small angles, and any method of preventing their entrance into the detectors would greatly simplify the experiment.

This reduction of proton background was desirable for the experiments we hoped to perform. The work of Daehnick[26] at Pittsburgh led us to suspect that proton induced, heavy particle differential cross sections could well be in the micro-barn/steradian region, or even less. These reactions could easily be masked by pile-up effects, or loss of counts due to detector and electronic dead time, and it was decided to try to reduce the proton level with an electrostatic separator.

An electrostatic separator (or analyzer) is simply a device by which charged particles are deflected by an electric field. The field is usually produced between a pair of parallel electrodes, and the geometry of the electrodes defines the field (linear, cylindrical or spherical, etc.). Only linear and cylindrical fields will be considered here.

The case of a linear field is quite simple and has seen extensive application in high energy physics.[27,28,29]

The equations of motion for a normally entrant particle of charge Ze, mass m, and energy T in an electrostatic field are

$$m \ddot{x} = 0$$

$$m \ddot{y} = ZeE$$

where x and y are coordinates defined in Figure 7, x being perpendicular and y parallel to the field direction. Solving these equations and eliminating the time, the deflection at any point x is

$$y = \frac{ZeEx^2}{4T} \qquad 4.1$$

and the angular deflection is

$$\tan \theta = \frac{ZeEx}{2T} \qquad 4.2$$

where θ is defined in Figure 7.

The separation of two particles (charge Z_1e, Z_2e and energy, T_1, T_2) is given by

$$y_1 - y_2 = eEx^2 \left(\frac{Z_1}{4T_1} - \frac{Z_2}{4T_2} \right) \qquad 4.3$$

and thus particles of different Z/T can be separated.

Relativistic corrections were not too important since $\beta^2 = 0.01$ for 25 MeV alpha particles and about 0.1 for 50 MeV protons, where β is the ratio of the particle velocity to the velocity of light.

FIGURE 7

LINEAR SEPARATOR GEOMETRY

FIGURE 8

CYLINDRICAL SEPARATOR GEOMETRY

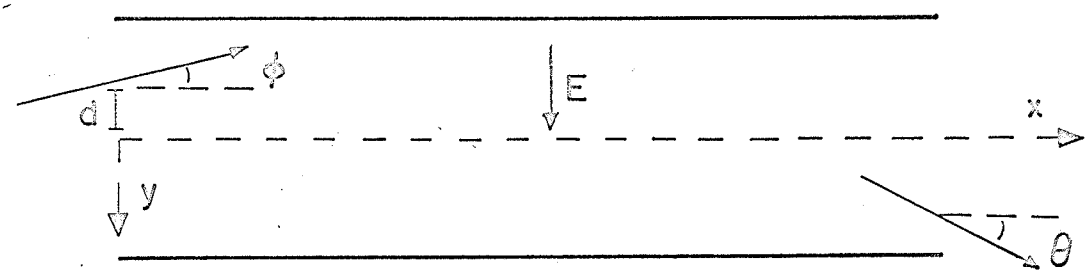
φ
d
E
x
y
θ

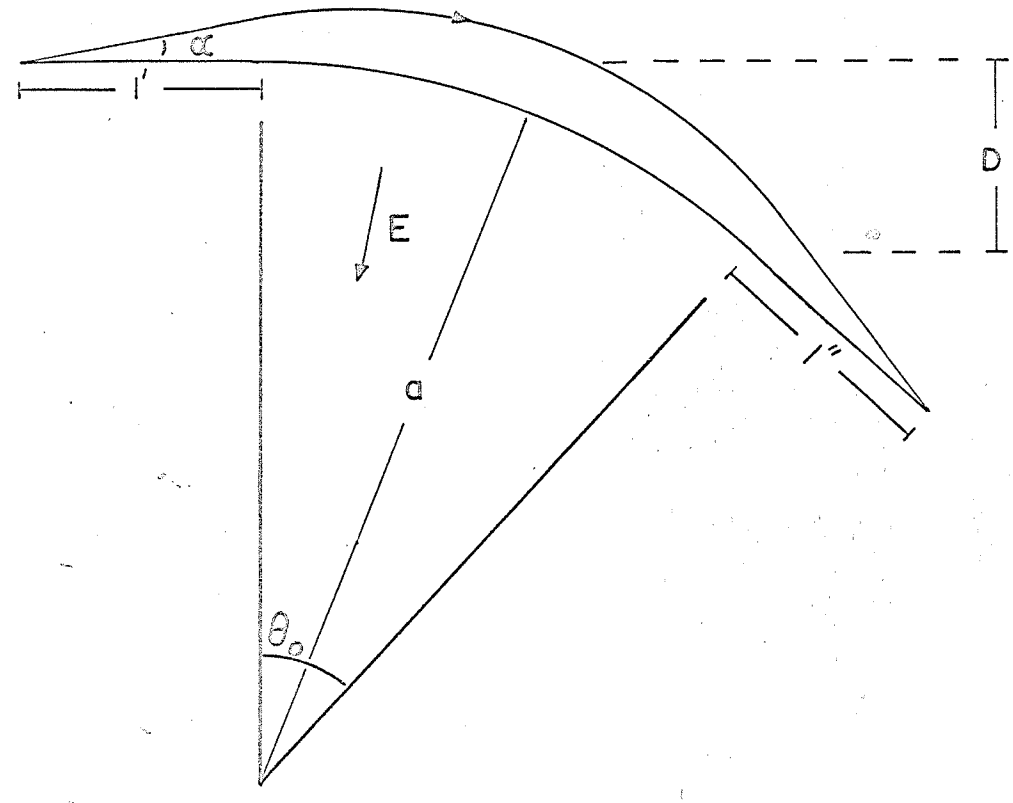
α
l'
D
E
a
l''
θ₀

If the particle is not normally entrant at y = 0, the equations are readily modified. If ϕ is the entrance angle and d the distance from the x axis, then

$$y = \frac{ZeE}{4T} \frac{x^2}{\cos^2\phi} - x \tan\phi - d \quad . \qquad 4.4$$

The deflecting and focusing properties of cylindrical electrostatic fields are well reviewed in the literature and only a brief outline will be presented here. Herzog[30] has developed a theory giving particle trajectory solutions in terms of image points and widths, and has demonstrated a complete parallelism with geometrical optics.

Referring to Figure 8, if the field region is defined by the angle θ_o, and if a is the radius of the separator, then Herzog[30] has shown that particles having small energy dispersion and entrance angle (α) satisfy the focusing condition

$$(l' - g)(l'' - g) = f^2$$

where

$$g = \frac{a}{\sqrt{2}} \cot\sqrt{2}\,\theta_o \quad ,$$

$$f = \frac{a}{\sqrt{2}} \csc\sqrt{2}\,\theta_o$$

and l' and l'' are the image and object distances respectively. Particles transmitted on the central axis of the separator satisfy the equation of motion

$$\frac{mv^2}{a} = ZeE$$

or

$$T = \frac{ZeEa}{2} \qquad 4.5$$

where m is the mass of the particle of velocity v and energy T, Ze is the particle charge, and E is the electric field.

If the separator radius is large with respect to the plate separation and object distance, and if the angular extent, θ_o, is small (less than 10^o) then the cylindrical results of Herzog reduce to those for a linear separator. Under these conditions, it can be shown that the object distance l" is given by

$$l'' \cong -l' - L$$

where l' is the image distance and L is the separator arc length, and thus the object and image points overlap as they must for a linear separator.

It can also be shown that the particle deflection D (Figure 8), for a cylindrical separator of slight curvature, is approximately the same as the deflection in a linear separator (equation 4.1) having the same length and electric field.

Design Restrictions

Equations 4.1 to 4.4 clearly show that the separation properties of a linear electrostatic analyzer improve with increasing length and field. A cylindrical separator is a more compact instrument with focusing properties, but its performance also improves with increasing field (decreasing radius) and length.

The largest scattering chamber available at the University of Manitoba was a 46 inch diameter tank and the highest voltage source was a 70 kV power supply. This meant that the separator length could not exceed about 50 cm and the gap width would have to be less than 1.0 cm for high fields.

Under these restrictions, the choice of separator design was critical and it was decided that tests must first be done to determine what fields could be obtained.

Electrode Surface

Early in their development, electric separators were constructed with highly polished conducting plates, usually stainless steel to avoid spark damage, and the upper limit to the fields was about 100 kV/cm.

Recently, a number of separators have been constructed with insulating cathode coatings. The impetus for their development was based on the fact that electric fields

of the order of several million volts per cm can be maintained across good dielectrics in a vacuum for very small gap widths. The basic idea is summed up by Murray:[31]

"The motivating idea was that a limiting class of vacuum sparks might involve in their incipient stage the emission of electrons from very small areas of the surface of the cathode at the eventual spark site, and if the bulk resistivity of the cathode were high enough, the degenerative effect of the local voltage drop at the emitting site would stave off or prevent an instability, whatever its nature might be, which would otherwise cause a spark."

Murray chose heated glass cathodes and was able to attain fields as high as 1000 kV/cm for gap widths of the order of 0.05 cm and hemispherical anodes. On an actual separator, the fields were the order of 200 kV/cm.

The effects of other insulating coatings will be considered later.

Results of CERN Group

It is now worthwhile to examine some high voltage work done at CERN by Rohrbach[32] since this important information is not readily available in the literature. Breakdown tests were performed across various flat electrodes (glass and oxide coated aluminum cathodes, and aluminum and stainless steel anodes) as functions of gap distance (1 to

10 cm) and pressure (10^{-6} to 10^{-3} torr). Electric fields of 62 to 190 kV/cm were obtained even after a large number of sparks.

The stainless steel plates were 10 mm thick AISI 304 and were mechanically polished and cleaned with trichlorethylene and alcohol. Three types of aluminum plates were used: 99.99% Al, 99.69% Al and an alloy of aluminum with 3% Mn. The electrodes were first mechanically polished, then polished with a velvet pad to ensure smoothness. The cleaning was done in the same way as for the stainless steel plates. In addition, some of the aluminum plates were given an insulating coating by sulphuric acid oxidation at $4^{o}C$ or at $20^{o}C$, resulting in hard or soft coatings respectively. The thickness of alumina varied from 1 to 100 microns, depending on the tests.

Before breakdown tests were attempted, a period of "low pressure conditioning" was required. During this time, the voltage was slowly raised and the gap current and sparking were allowed to settle down to a constant low level. This was done when the pressure reached 10^{-6} torr in the vacuum tank.

The pressure in the tank was then slowly raised by a controlled injection of gas and the breakdown voltage was noted. A small dispersion in values of voltage was noted for breakdown between the plates but a much larger dispersion resulted after damage to the plate support systems. This

damage was due mainly to excessive sparking or eventual external contamination (presumably organic vapors). In general, the breakdown voltage increased with increasing pressure, to a maximum just before complete breakdown at about 5×10^{-4} torr. Moreover, this pressure effect is greater the larger the gap. At the critical pressure, excessive sparking is accompanied by gaseous Paschen discharge.

The above procedure was followed for various gap distances and for various electrodes. Rohrbach found that when the pressure effect is considered, the voltage gap law ($V = Kd^a$; K, a are constants) is not strictly correct. However, log V - log d plots are almost linear and their mean slopes are nearly the same ($a = 0.62 \pm .09$) for all metallic electrodes. This indicated that the breakdown process is probably similar for these electrodes. For gap distances of less than 3 cm the oxide coated electrodes seemed to give irregular results.

The effect of the kind of electrode on voltage breakdown is shown in Table 1. The values of the maximum electric field E, in kV/cm, correspond to the breakdown voltage at the optimum pressure (the critical pressure is about 5×10^{-4} torr). Complete breakdown occurs here.

From this table it is obvious that soft oxide coated aluminum cathodes give the highest fields. Low oxide bath temperatures ($4^{\circ}C$) give the hardest coatings, but these craze rapidly with sparking and this causes more

TABLE 1 CERN RESULTS ON INFLUENCE OF ELECTRODES ON VOLTAGE BREAKDOWN (5.0 cm gap)

Test #	Cathode		Anode		Max E kV/cm
	Metal	Electrode Surface	Metal	Electrode Surface	
1	99.69% Al	natural oxide	Inox.304	untreated	138
2	99.69% Al	1.5-3 μ soft oxide layer	Inox.304	untreated	156
3	99.69% Al	4-7 μ soft oxide layer	Inox.304	untreated	162
4	Al + 3% Mn	9-10 μ soft oxide layer	Inox.304	untreated	158
5	99.69% Al	4-7 μ soft oxide layer	99.69% Al	natural oxide	190
6	99.69% Al	25-30 μ soft oxide layer	Inox.304	untreated	148
7	99.69% Al	92-102 μ hard oxide layer	Inox.304	untreated	96
8	Inox.304	untreated	99.69% Al	25-30 μ hard oxide layer	62
9	99.69% Al	natural oxide	99.69% Al	natural oxide	134
10	Inox.304	untreated	Inox.304	untreated	97
11	Al + 3% Mn	5-6 μ soft oxide layer	Inox.304	untreated	164
12	99.99% Al	5-7.5 μ soft oxide layer	Inox.304	untreated	144
13	99.69% Al	25-30 μ hard oxide layer	Inox.304	untreated	142
14	99.69% Al	7-10 μ hard oxide layer	Inox.304	untreated	128
15	Al + 3% Mn	1.5-2.5 μ soft oxide layer	Inox.304	untreated	154

sparks. The uncoated aluminum electrodes give higher fields than uncoated stainless steel but this is probably due to the natural oxide layer always present on aluminum. The optimum thickness for this oxide layer seems to be about 5 microns.

It is also evident that the type of aluminum electrode used is unimportant. The type of anode, however, is quite important. Aluminum anodes (and cathodes) give the highest fields (190 kV/cm) but after a few weeks, these anodes are irreversibly damaged by sparking. The anode surface is pitted with large craters and the breakdown voltage decreases continually. Stainless steel anodes however, stand up very well. Interchanging the electrodes results in much lower fields.

It is worth noting that the performance of the glass coated electrodes was not as good as for the metallic electrodes. The maximum electric fields obtainable were about 120 kV/cm.

Breakdown Tests

The results of the CERN group indicated that soft oxide coated aluminum cathodes and stainless steel anodes give the best results for gap distances greater than 3.0 cm. For this arrangement, the maximum electric field attained was about 160 kV/cm.

It was decided to try and reproduce Rohrbach's results for the following reasons: to find the maximum breakdown voltages for less sophisticated electrode support systems; to find the critical pressure at which complete breakdown occurs (Rohrbach indicated that this depended on vacuum chamber shape etc.); and to test the effect of sparking with oxide coated aluminum for gap distances less than 1.0 cm. The latter reason is of particular importance since the CERN group had erratic results at these small gap distances. We were limited to a 70 kV voltage supply and thus would have to go to gap distances of about 0.4 cm to attain a field of 160 kV/cm.

Three basic types of electrodes were investigated: spherical stainless steel anode and cathode (0.625 inch diameter); 0.25 inch thick flat stainless steel anode and cathode (9 $in.^2$); and 0.25 inch thick flat stainless steel anode (9 $in.^2$) with a 0.25 inch thick flat oxidized aluminum cathode of circular shape (2 inch diameter).

The electrodes were polished to a high gloss by hand and cleaned in trichlorethylene and alcohol.

The aluminum cathode was oxidized in a sulphuric acid bath (20% by weight) at 20°C to produce a soft oxide layer. The thickness of the alumina was determined by the oxidation time, and preliminary breakdown tests set the optimum time at about 5 minutes. Finally, the coating was sealed in a hot (about 100°C) distilled water bath.

The various electrodes were interchangeable and a facility for varying gap distances was available. The test assembly is shown in Figure 9.

The effect of electrode shape and surface coating is shown in Table 2. In all cases, the critical pressure at which complete breakdown occurred was between 5×10^{-5} torr and 10^{-4} torr and as this critical pressure was approached the breakdown voltage decreased.

All tests were preceeded by a period of low pressure conditioning. That is, the voltage was raised slowly until sparking and gap current fluctuations settled down. This was done at pressures around 2×10^{-6} torr.

No exhaustive attempt was made to test the approximate voltage - gap distance law, $V = Kd^a$ (K, a constants), since the difference in gap distances were small. However, the results of tests 8, 9 and 10 give $a = 0.50 \pm .15$ which agrees with the CERN results. It can be concluded therefore, that for best results, the gap should be as small as possible, consistent with reasonable counting rates.

The tests clearly show the effect of build up of contamination on the plate support systems. The maximum fields of tests 2, 3 and 4 were about half that of test 1 for identical geometry and were limited by arcing from the supports to the chamber wall. Tests 6 and 7 show a similar effect. This was caused by excessive sparking and continual

FIGURE 9

BREAKDOWN TEST APPARATUR

A High Voltage Inlet
B Beam Pipe
C Anode Advance
D Plates

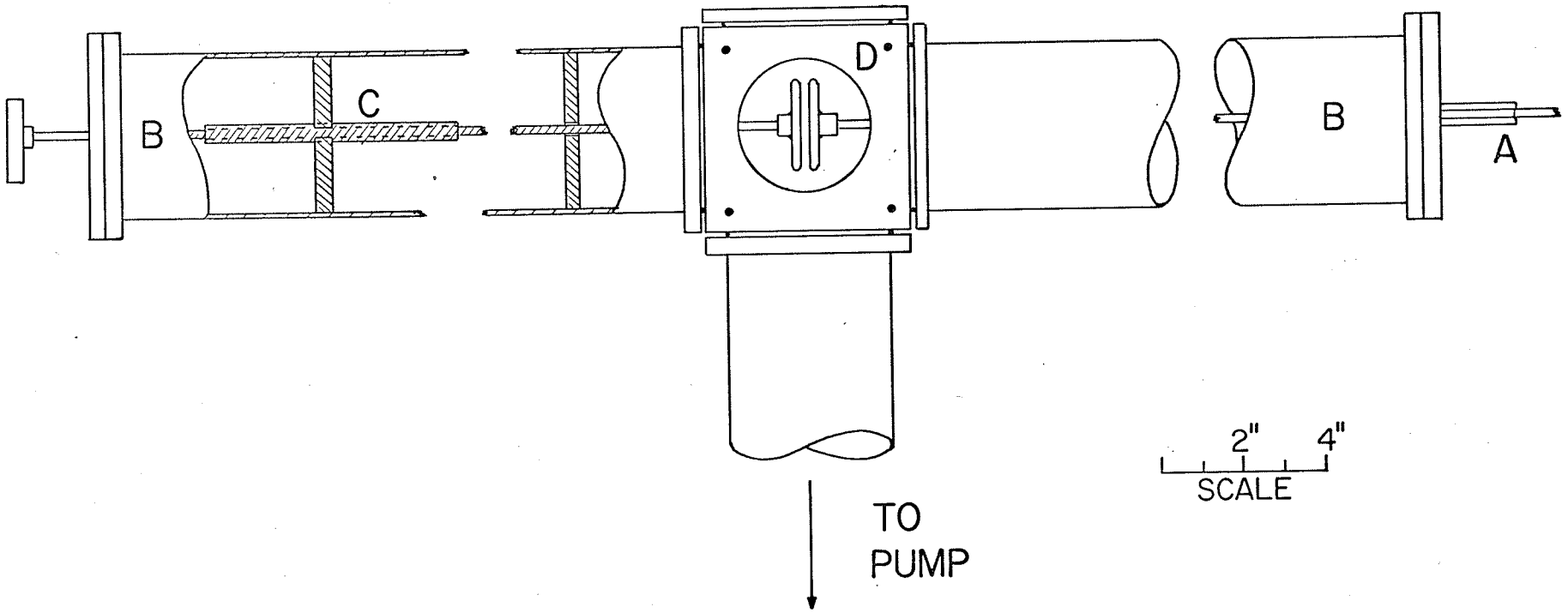
B
C
D
B
A
2"
4"
SCALE
TO
PUMP

TABLE 2 INFLUENCE OF ELECTRODES ON MAXIMUM FIELD OBTAINED

Test #	Cathode		Anode		Gap cm	Max E kV/cm	Spark Rate /min
	Metal	Electrode Surface	Metal	Electrode Surface			
1	Stainless Steel	spherical, untreated	Stainless Steel	spherical, untreated	0.17	390	-
2	Stainless Steel	spherical, untreated	Stainless Steel	spherical, untreated	0.20	200	-
3	Stainless Steel	spherical, untreated	Stainless Steel	spherical, untreated	0.27	204	-
4	Stainless Steel	spherical, untreated	Stainless Steel	spherical, untreated	0.31	195	-
5	Stainless Steel	flat, untreated	Stainless Steel	flat, untreated	0.26	100	-
6	Stainless Steel	flat, untreated	Stainless Steel	flat, untreated	0.26	75	-
7	Stainless Steel	flat, untreated	Stainless Steel	flat, untreated	1.00	55	-
8	Aluminum	flat, soft oxide layer 8 min oxidation time	Stainless Steel	flat, untreated	0.74	92	1/7
9	Aluminum	flat, soft oxide layer 5 min oxidation time	Stainless Steel	flat, untreated	0.50	115	1/5
10	Aluminum	flat, soft oxide layer 4 min oxidation time	Stainless Steel	flat, untreated	0.61	95	1/10
11	Aluminum	flat, soft oxide layer	Stainless Steel	10-24 Allan bolt	2.54	Breakdown V = 68kV	
12	Aluminum	flat, soft oxide layer	Brass	Irregular	2.54	Breakdown V = 48kV	

venting of the system. The effect was sometimes reduced by venting followed by low pressure conditioning (if done soon enough). Failing this, the entire electrode support system had to be thoroughly recleaned. It was concluded that the support system was not too critical, provided it was smooth, clean, and free from irregular edges.

The results show that spherical stainless steel electrodes gave fields up to 390 kV/cm for gap widths of 0.17 cm. Flat stainless steel electrodes produced 75 kV/cm to 100 kV/cm fields at 0.26 cm gaps. Finally, the best arrangement - stainless steel anode and soft oxide coated aluminum cathode - gave fields between 100 kV/cm and 115 kV/cm over the range of gap widths of interest (those consistent with reasonable counting rates). The spark rate was about 1 per 7 minutes.

In addition, tests 11 and 12 were done to determine the minimum distance irregular objects could be placed near the plates to avoid arc over. This minimum distance seems to be about 1.5 inches.

Final Design

The results of the breakdown tests indicated that electric fields of 100 kV/cm could be maintained for long periods of time across stainless steel anodes and oxide coated aluminum cathodes. This result, together with the design restrictions mentioned earlier, completely ruled out any

configuration of a linear electrostatic separator. For a reasonable separation of the order of 1 or 2 cm for Z = 1 and 2 particles of 30 MeV, the electric field required is 85 kV/cm (see equation 4.3). At this field however, the gap width must be 0.8 cm and thus charge 2 particles are lost in the plates. In addition, the electric field limitation ruled out a short separator of very high field.

It was decided, therefore, to build a cylindrical separator and for flexibility, a variable radius type was chosen. The final design is shown in Figure 10. The length was made 40 cm (actually 39.8 cm) so that sparking would not occur between the separator and target holders or detectors (see Table 2). The gap width was 0.67 $\pm$ .05 cm, but when the plates were bent, the narrowed to a mean value of about 0.63 cm. The anode support system was constructed with a 1.91 cm gap along the median horizontal plane of the separator so that the proton beam would not intersect the support system at small angles - angles between 10^{o} and 170^{o} could be investigated. In addition, perspex insulators were used throughout.

The anode was constructed of stainless steel and the cathode was aluminum. The electrodes were cleaned in trichlorethylene and alcohol and the cathode was oxidized to produce an optimum thickness of alumina as described previously for the test electrodes.

The plates were fixed at the separator entrance and

FIGURE 10

THE ELECTROSTATIC SEPARATOR

A Fixed End

B Movable End

C Plate Bending Screw

D Al Cathode

E Stainless Steel Anode

F Cathode Support (Perspex)

G Anode Support (Steel)

H High Voltage Terminal

I Gap

J Fixed Support Table

TOP VIEW

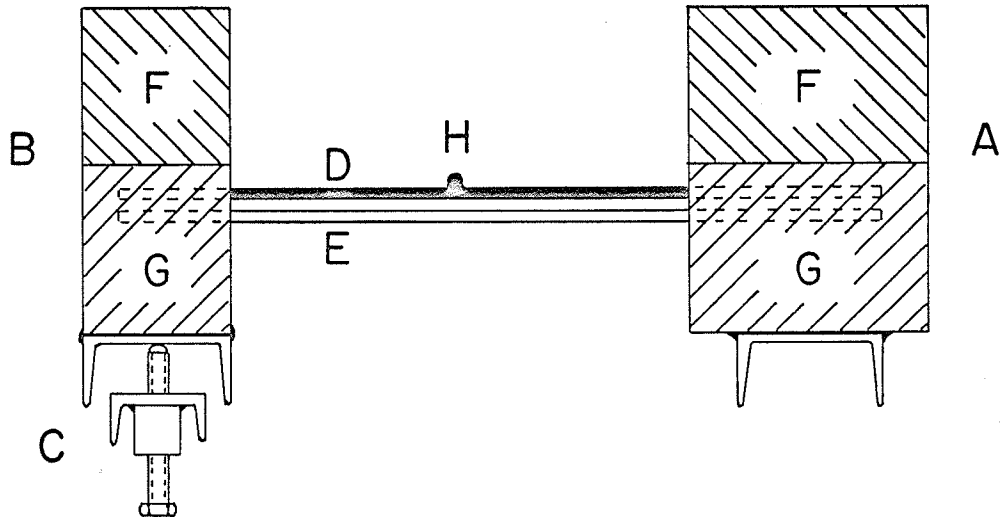

SIDE VIEW
(Screw not shown)

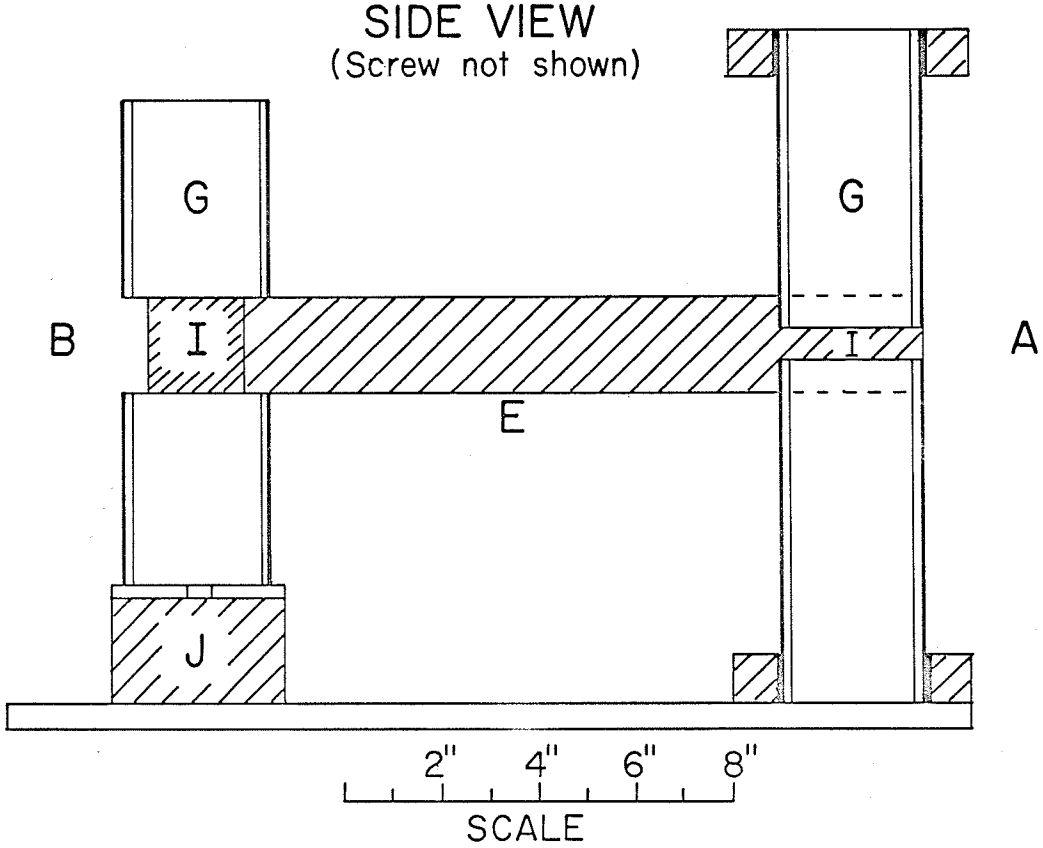

the radius was varied by bending both plates with a screw mechanism at the separator exit.

The gap width was made 0.63 cm so that the maximum field could be attained and the field was found from the approximate relationship E = (V/0.63) kV/cm. This approximation was considered quite good since the separator radius was of the order of 300 to 500 cm.

The radius and field were related through equation 4.5 and for this separator took the form

$$T = \frac{Z}{1.26 \times 10^3} aV \qquad 4.6$$

where the energy T was in MeV, the radius a in cm, and V in kV. The radius and voltage could be varied to provide optimum separation of various heavy reaction particles from the proton background.

The system had no net focusing or defocusing properties. The maximum electric field attainable limited the radius to a minimum value of about 300 cm and the chamber size and separator radius limited the angular extent to about 7°. Using the deflecting and focusing equations discussed earlier (p. 37) resulted in a focal length of the order of 1300 cm and since object distances were about 5 cm, the image was virtual. For an exit deflection of 2.5 cm (radius = 316.8 cm), and an object distance of 5.08 cm, the image distance was -43.2 cm; an exit deflection 2 cm (radius =

396.0 cm) resulted in imaging at -45.1 cm. Both virtual images overlapped the object site (at -44.9 cm in image distance coordinates) within 2 cm and thus no defocusing occurred.

This lack of focusing or defocusing meant that image sizes could be calculated geometrically, and that the separator could be approximated by a linear separator for ease in calculating particle trajectories (pp. 37 and 38).

Some calculations were done to get an approximate idea of the probability of proton scattering from the separator plates into the detectors. This probability was of the order of 10^{-3} to 10^{-6} and was considered negligible.

Separator Tests

Preliminary breakdown tests were done on the completed separator and indicated that fields of about 75 kV/cm could be maintained for long periods of time with spark rates of the order of 10 to 15 per minute. At 60 kV/cm, no sparking occurred.

The transmission properties were tested with 5.5 MeV alphas from an Am^{241} source and the results are shown in Figure 11. The transmission of alpha particles from a (p,He^4) reaction in C^{12} is discussed in Chapter 7. The alpha source was placed 25 cm in front of the separator and the number of counts under the peak was recorded as the voltage was raised. Tests were done with and without collimation 5 cm before the separator and no significant differences were

FIGURE 11

SEPARATOR TRANSMISSION FOR
Am^{241} ALPHAS AT 5.48 MeV

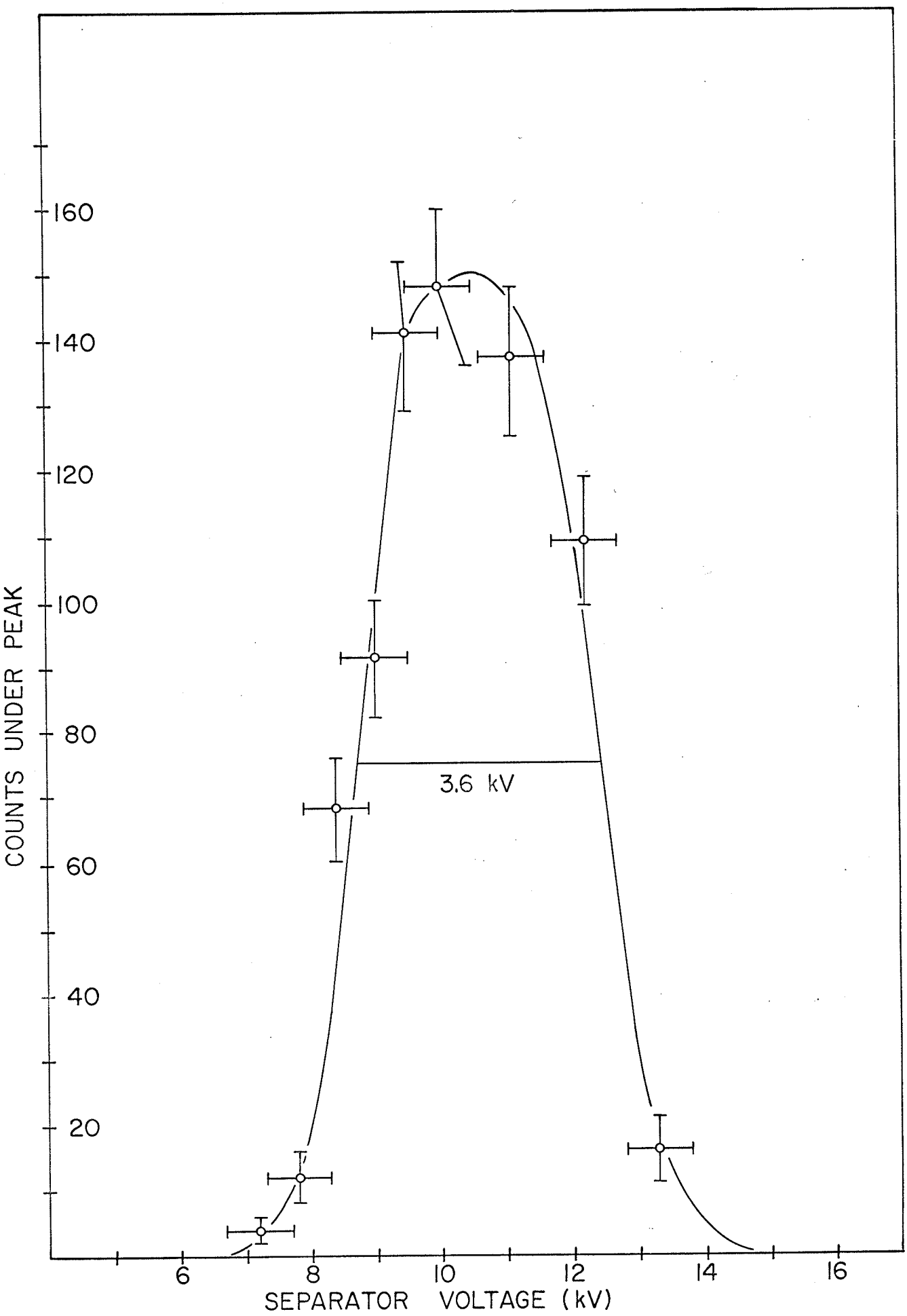
160
140
120
100
80
60
40
20
COUNTS UNDER PEAK
3.6 kV
6
8
10
12
14
16
SEPARATOR VOLTAGE (kV)

found in the widths or positions of the distributions. The separator radius was 318 cm, corresponding to an exit deflection of 2.5 cm, and the calculations (equation 4.6) indicated that the transmission peak should occur at 10.9 kV. The experimental peak occurred at 10.4 $\pm$ 0.5 kV and this agrees with the predicted value. These results, together with later experimental evidence (Chapter 7), showed that the optimum voltage for transmission of a given particle, at a given energy, could be calculated quite accurately.

The ratio of the number of counts observed at the transmission peak to the number calculated geometrically was about 1.1, but the errors involved were between 5% and 10% and it was concluded that there was no significant difference between the theoretical and experimental results.

CHAPTER 5 THE ELECTRONICS

Particle Identification

Most particle identification techniques involve energy analysis in conjunction with simultaneous analysis of a second parameter. Such things as magnetic rigidity and time of flight have been used,[26] but the second parameter we chose was the energy loss in the proportional counter.

Various electronic techniques have been employed to handle the dE/dx and E pulses and thus obtain the particle identification, but only two will be considered here.

The first involves Bethe's energy loss formula previously mentioned (p. 5):

$$-\frac{dE}{dx} = \frac{2\pi e^4 Mz^2}{mE} NZ \ln\frac{4mE}{MI}$$

where m is the electronic mass, ze is the charge of the particle of mass M, and N is the atomic density, Z the atomic number, and I the average atomic excitation potential of the stopping material.[10] A multiplier circuit is used to find the product (dE/dx)E and this is proportional to Mz^2 if the nearly constant logarithmic term is neglected. This system has seen extensive applications[33,34] despite the fact that (dE/dx)E vs. E plots are not quite energy independent.

A more sophisticated procedure is to approximate the effect of the logarithmic term by assuming that a

quantity $P = (E + K\Delta E + E_o)(dE/dx)$ is energy independent and proportional to $Mz^{2.35}$ [35] E_o and K are adjustable parameters generated in the circuit. The output P then gates a pulse height analyzer. This method is quite good and gives results comparable to the logarithmic method discussed below. The peak to valley ratios of p to d, and d to t in the mass spectrum are about 100/1 and 10/1 respectively.

Another technique utilizes the range-energy relation,

$$R = aE^b$$

and for the lighter reaction products between 5 and 50 MeV, b is about 1.73; a is a constant and is particle dependent. If the energy loss of a particle in the thin detector (thickness = t) is dE, and in the total energy counter is E (range = R) then

$$R + t = a(E + dE)^{1.73}$$

and

$$R = aE^{1.73}$$

Thus

$$(t/a) = (E + dE)^{1.73} - E^{1.73}$$

and by proper logarithmic handling of the counter outputs, the identifier output can be made proportional to (t/a). This system has excellent identifying characteristics.[36,37]

It was decided that neither of these methods would be employed for heavy particle reactions at the initial stage of investigation. For a first experiment, it seemed simpler to use a direct method. This technique consisted of displaying E on one axis and ΔE on the other axis of a two dimensional analyzer and observing the hyperbolic loci corresponding to various values of Mz^2.

Counter Systems

The electronics associated with the counters and identifying systems are shown in Figure 12. Adequate shielding and low inductance grounds were used throughout to minimize ground loop effects and noise pickup in the experimental area. The long cables from the experimental to control room areas introduced similar problems and all preamplifiers were used at maximum gain settings to boost the pulses well above this noise level. This necessitated the use of a variable attenuator and an amplifier to display the total energy pulses properly at the pulse height analyzer.

The proportional counter pulses were monitored in the experimental area with an oscilloscope so that the proper operating region could be determined every time the argon gas was changed. In addition, the pulse heights from an alpha calibration source were continuously monitored in the control room to check for drift.

The proportional counter pulses were directed to

FIGURE 12

THE ELECTRONICS

P.S. means Power Supply

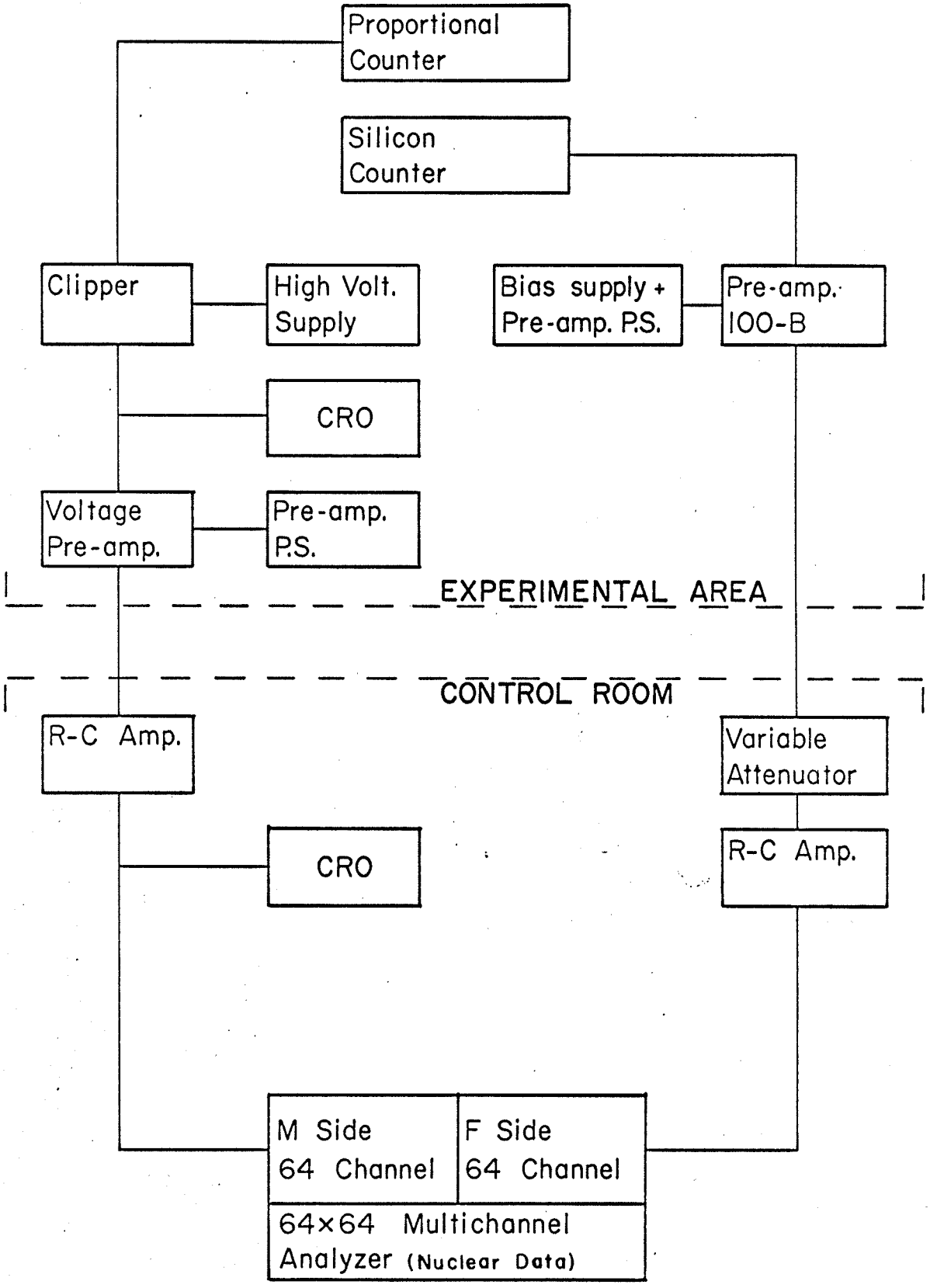
Proportional Counter
Silicon Counter
Clipper
High Volt. Supply
Bias supply + Pre-amp. P.S.
Pre-amp. 100-B
CRO
Voltage Pre-amp.
Pre-amp. P.S.
EXPERIMENTAL AREA
CONTROL ROOM
R-C Amp.
Variable Attenuator
CRO
R-C Amp.
M Side 64 Channel
F Side 64 Channel
64×64 Multichannel Analyzer (Nuclear Data)

the M side (ordinate) of the Nuclear Data (64 x 64 channel) two dimensional analyzer and the silicon counter pulses were fed to the F side (abscissa). Provision was made within the analyzer to change the address system and convert to 128 x 32 or 256 x 16, etc. operation if better resolution was required at the F side. The coincidence pulses displayed by the pulse height analyzer were the hyperbolic loci corresponding to different particles ($E(dE/dx)$ proportional to Mz^2).

As previously mentioned (pp. 6 and 7), any protons passed by the separator lost only a fraction of their energy in the E counter and thus identification of higher energy heavy particle peaks was fairly easy and not masked by the protons.

The data was punched on paper tape and the tape fed to a tape to typewriter converter to get a typed output. The resulting two dimensional spectra were analyzed by a contour method, where constant counts/channel were joined by contour lines on a 64 x 64 channel display.

CHAPTER 6 BEAM TRANSPORT SYSTEMS

The Cyclotron

The University of Manitoba cyclotron[38] (Figure 13) is a sector-focused type with a design energy of 50 MeV for protons. The magnet pole diameter is 46 inches and the maximum orbit radius is 21 inches. The magnetic field is trimmed by a network of temperature controlled Invar blocks.

The cyclotron accelerates negative ions (H^-) produced by a modified Oak-Ridge type negative ion source and the beam is extracted by a stripping process. The negative ions are stripped of their electrons by passage through a thin foil thus reversing the radius of curvature of their path, and the resulting protons are then deflected from the machine.

The energy of the proton beam may be varied by moving the stripping foil to smaller cyclotron radii resulting in a deflected beam of reduced energy. The deflected proton beam (maximum current about 1 μA) is steered into the beam pipe by a bending magnet at the main magnet yoke. In this manner, the energy may be varied from about 25 to 50 MeV.

The output proton beam is not, in general, strictly monoenergetic. When the magnet is tuned for maximum beam current, the beam energy spectrum shows multiple peaking (Figure 14). Detuning the magnet slightly (about 2%) changes the energy shape, however, and by an empirical detuning procedure it is possible to obtain a reasonably monoenergetic

FIGURE 13

THE CYCLOTRON AREA

1 CYCLOTRON
2 QUADRUPOLE–DUPLET
3 SCATTERING CHAMBER
4 FARADAY CUP
5 CONCRETE BLOCKS
6 VAULT DOOR
7 EXPERIMENTAL RM. DOOR
8 ACCESS SHAFT
9 EMERGENCY EXIT
10 HEAT EXCHANGER
11 WELL
12 MAGNET POWER SUPPLY
13 R.F. H.V. POWER SUPPLY
14 MAINS TRANSFORMER AND DISTRIBUTION PANEL
15 CROSS CONNECT RACKS
16 CONTROL CONSOLE
17 COUNTING EQUIPMENT

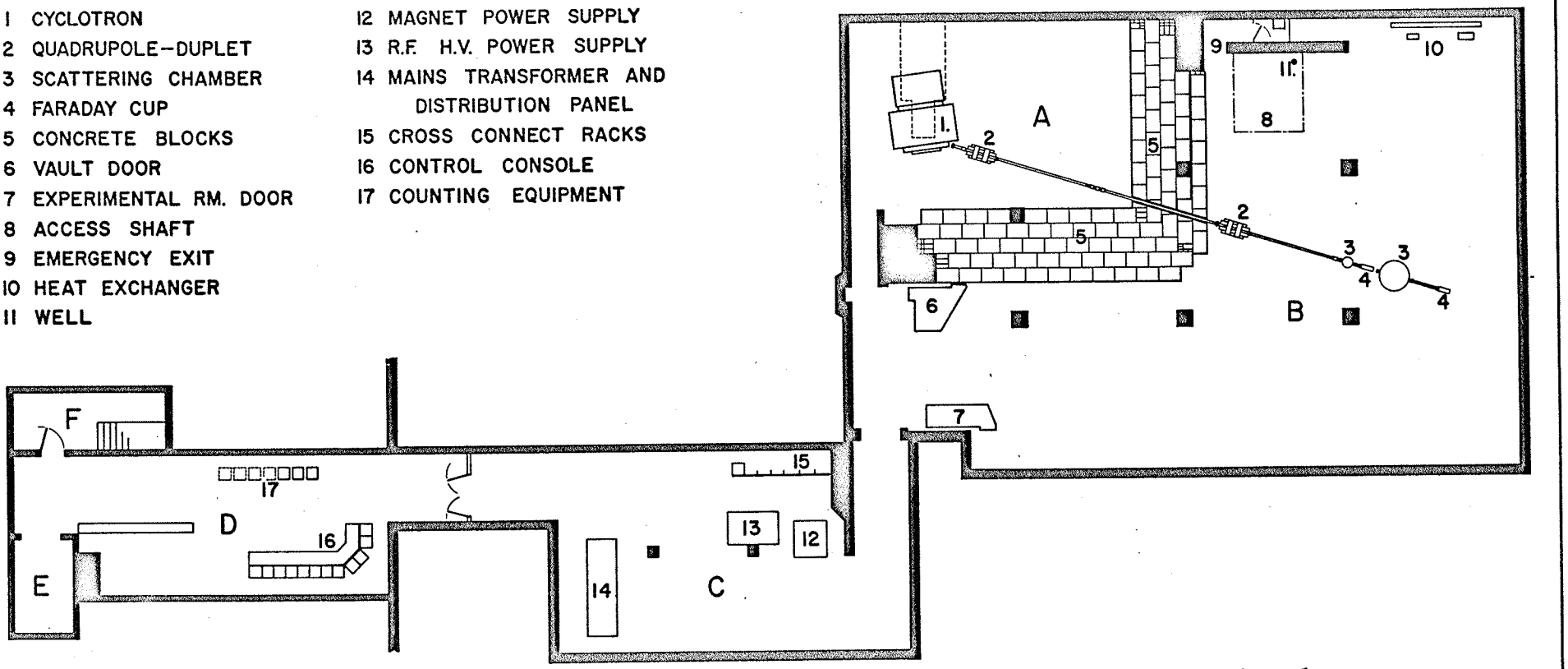

A CYCLOTRON VAULT
B EXPERIMENTAL AREA
C ELECTRICAL ROOM
D CONTROL ROOM
E ELEVATOR
F STAIR HALL

20 FEET

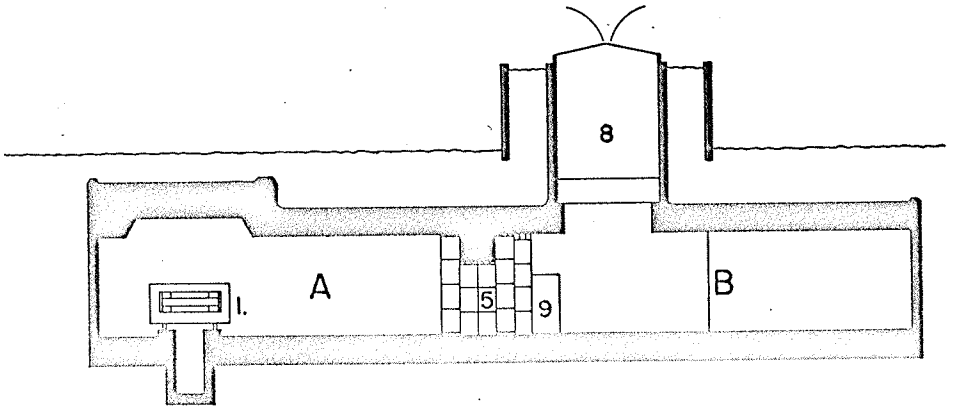

FIGURE 14

THE BEAM ENERGY SPECTRUM

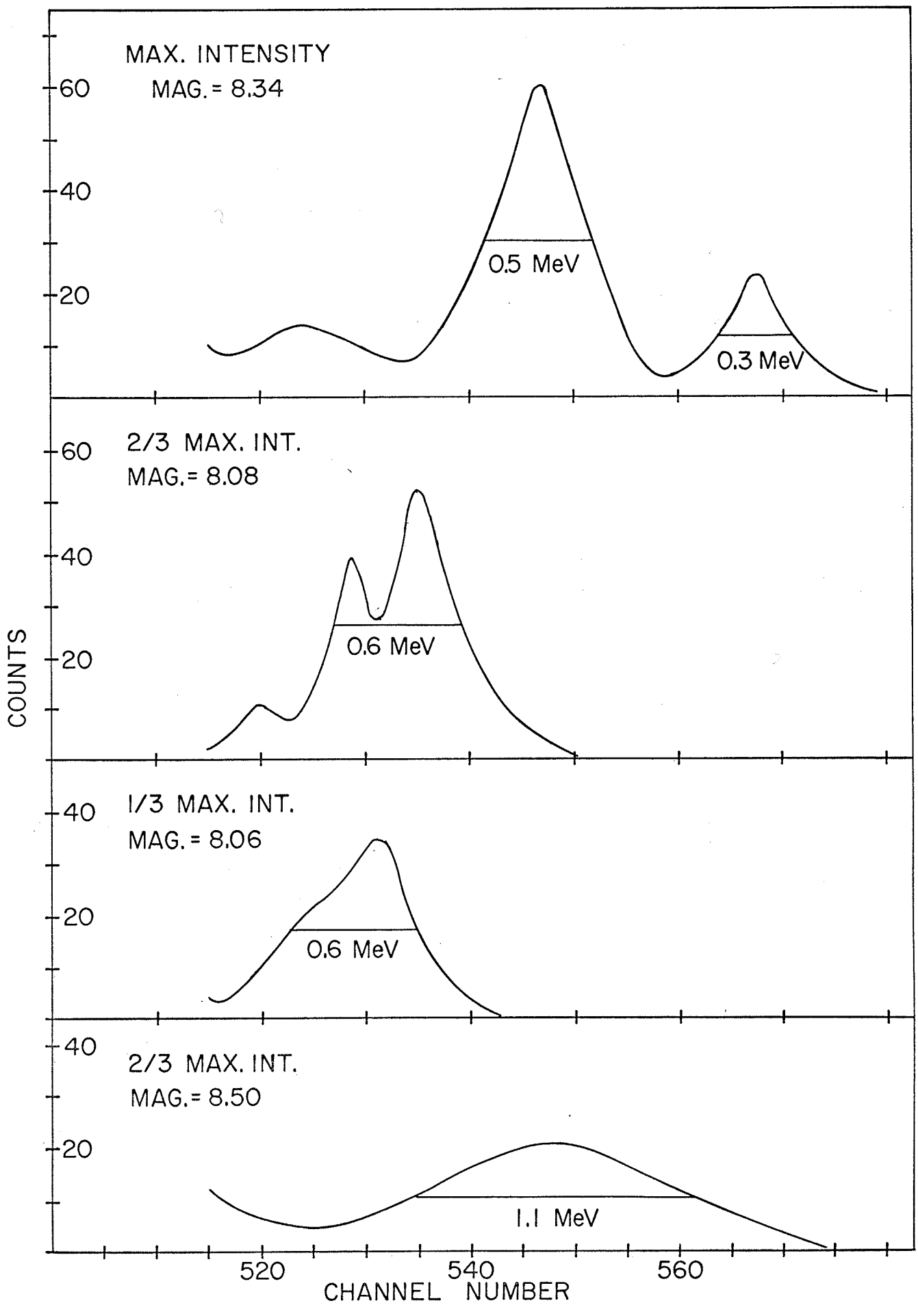
MAX. INTENSITY
MAG. = 8.34
60
40
20
0.5 MeV
0.3 MeV
2/3 MAX. INT.
MAG. = 8.08
60
40
20
0.6 MeV
1/3 MAX. INT.
MAG. = 8.06
40
20
0.6 MeV
2/3 MAX. INT.
MAG. = 8.50
40
20
1.1 MeV
COUNTS
520
540
560
CHANNEL NUMBER

proton beam. The energy shape depended on stripping foil position and angle as well as other machine parameters so that the exact energy shape was not reproducible from day to day. However, reducing the beam intensity to about 1/3 maximum by slightly detuning the magnet seemed to give satisfactory results in most cases.

Figure 14 shows a typical alpha energy spectrum from a $C^{12}(p,He^4)B^9_{g.s.}$ reaction as the proton beam intensity is varied by the magnet. The proton energy spectrum is reproduced in the alpha peaks. The apparatus used here was borrowed from another cyclotron group* to take advantage of the higher resolution of their detector systems. Our equipment yielded essentially the same results, but some of the multiple peaking was blurred out due to poorer resolution.

Beam Handling

The proton beam passed from the cyclotron to the scattering chambers through a 4 inch diameter beam pipe. Two pairs of quadrupole magnets focused the beam - the first focus at 24 feet from the stripping foil and the second at the center of the 46 inch diameter scattering chamber. The beam was collimated at the entrance of the scattering chamber and at the Faraday cup, where the beam current was measured.

The losses at the first collimator were typically 80% resulting in a beam current at the Faraday cup of about 0.1 μA maximum.

* with thanks to C. Kost, S.Y. Li and B. Hird, University of Manitoba

Scattering Chamber

Figure 15 shows the 46 inch diameter scattering chamber with the apparatus in place. The graphite entrance collimator was rectangular in shape, measuring 1.27 cm in the vertical direction and 0.64 cm horizontally, to take advantage of the rectangular geometry of the separator. The exit collimator was a 4 inch O.D. polyethylene plug with a 2 inch diameter aperture. The chamber was evacuated by a large mechanical pump (62.3 liter/sec capacity) and a Balzers diffusion pump.

A facility was available to rotate a base plate inside the chamber, and the apparatus was attached to this plate.

The targets were mounted on a rectangular brass target holder by gluing the foils over two fine nylon wires, 1.27 cm apart, as shown in Figure 15. This type of mount was used to reduce proton scattering from the target holder. The target holder was able to move up or down through a vacuum tight seal in a port at the top of the chamber.

The counter signal leads were brought out through connectors on the top port and the gas inlet for the proportional counter was through a vacuum-tight rotating seal at a port on the bottom of the chamber.

Photographs of the apparatus are shown on Plates 1 to 4.

FIGURE 15

THE SCATTERING CHAMBER AND APPARATUS

A Beam Pipe

B High Voltage Inlet

C Gas Inlet

D Gas Leads

E Separator

F Proportional Counter

G Solid State Counter

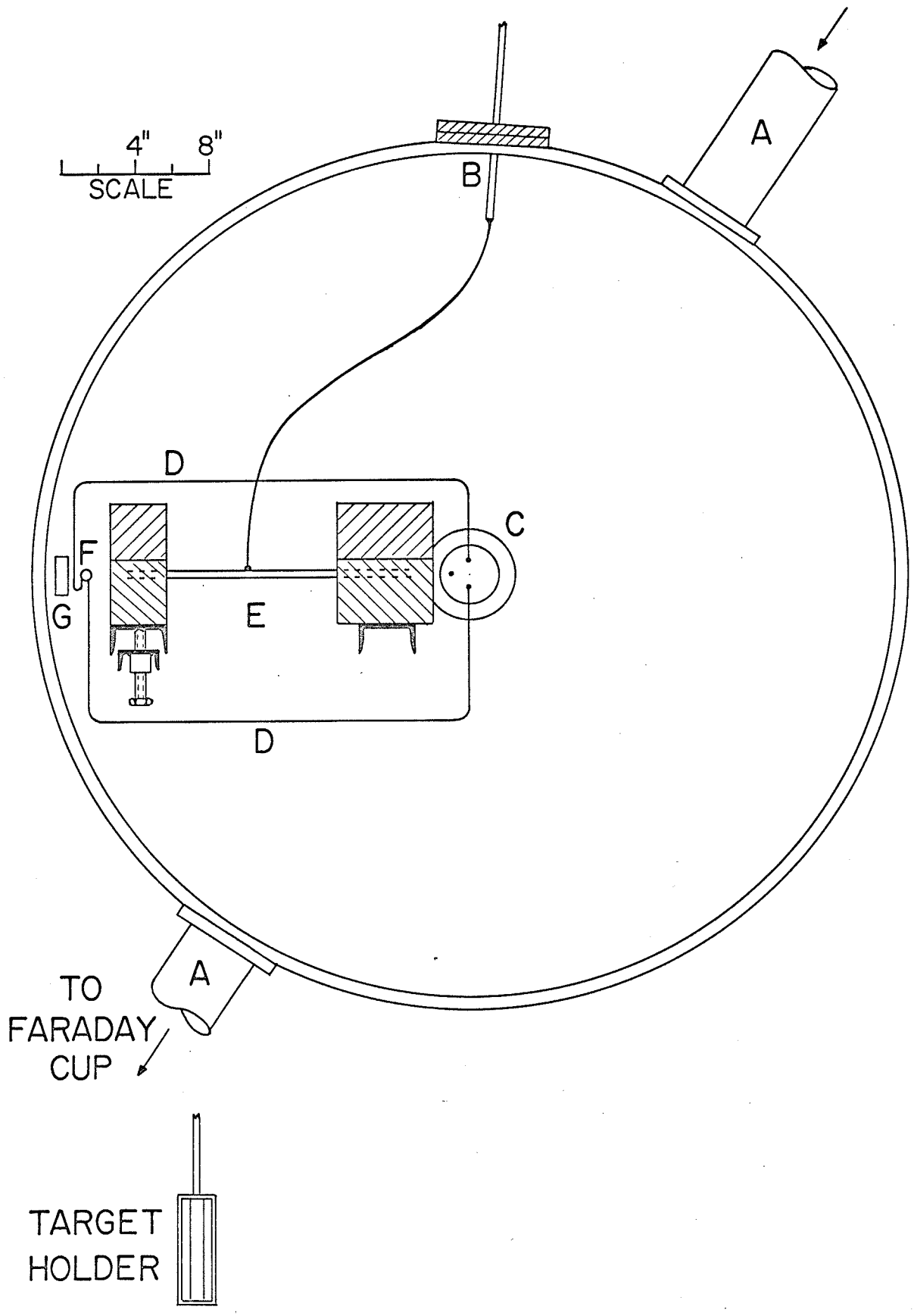
4"
8"
SCALE
A
B
D
C
F
G
E
D
A
TO
FARADAY
CUP
TARGET
HOLDER

PLATE 1

THE CYCLOTRON

PLATE 2

THE SCATTERING CHAMBER

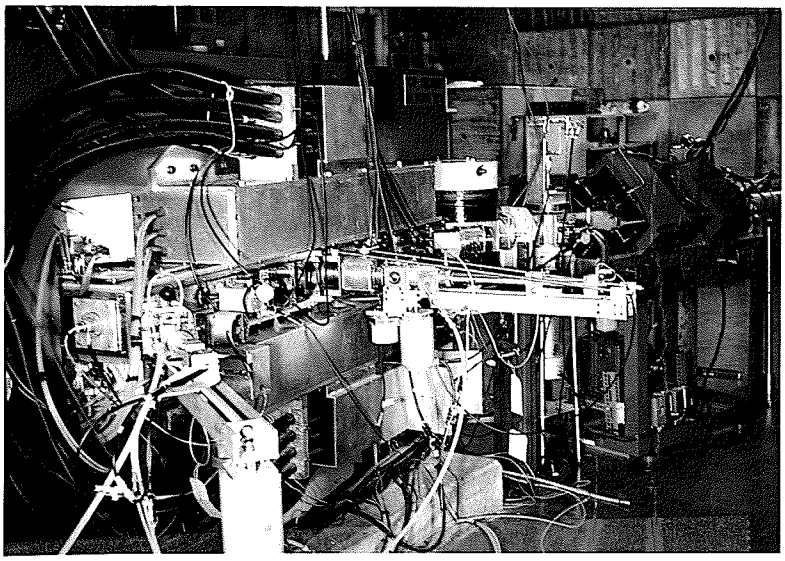

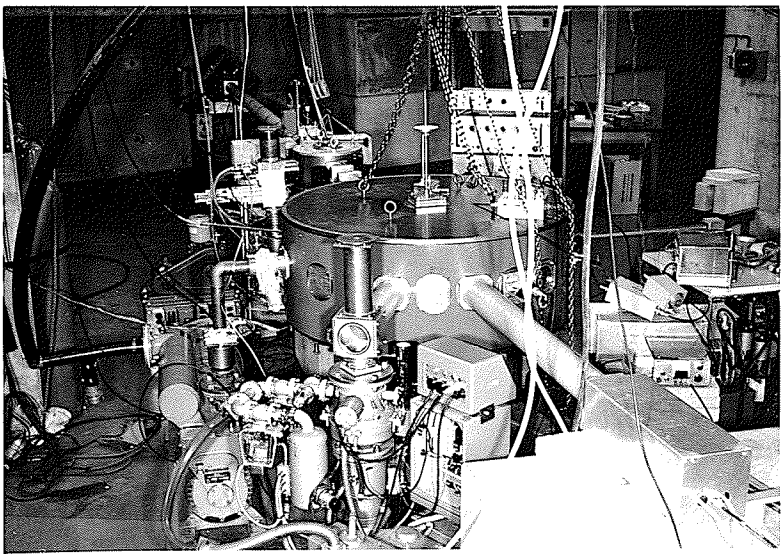

PLATE 3

THE ELECTROSTATIC SEPARATOR

PLATE 4

THE PROPORTIONAL COUNTER

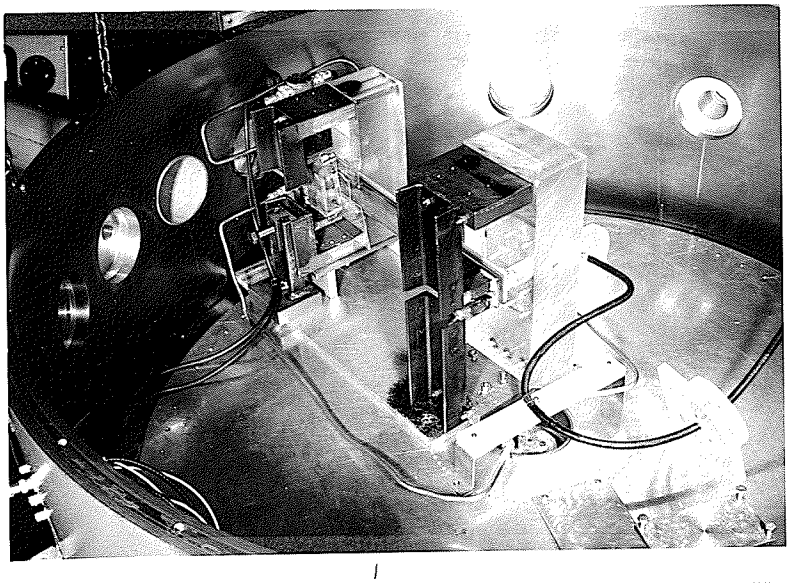

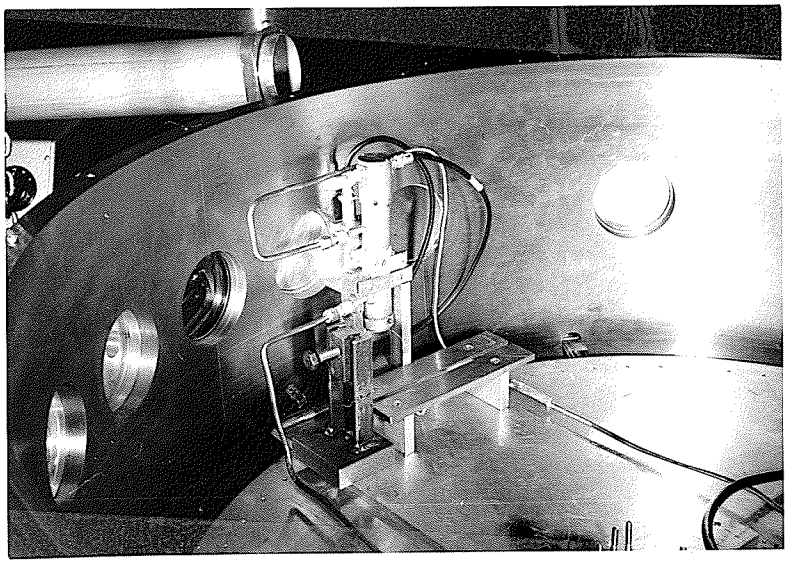

SECTION III THE RESULTS

CHAPTER 7 CALIBRATION OF EQUIPMENT

$C^{12}(p,He^4)B^9$ Coincidence Spectra*

The counter telescope system was calibrated with natural alphas (6.05 MeV from Bi^{212} and 8.78 MeV from Po^{212}) and alpha particles from the $C^{12}(p,He^4)B^9$ reaction. Since it was not possible to simultaneously analyze more than two adjacent z groups and still obtain reasonable resolution between the groups, owing to the limited number of channels on each axis of the 64 x 64 display, the proportional counter gain had to be varied to observe different groups. This meant that all calibrations were repeated each time the counter gains were changed.

The targets consisted of 1.91 cm by 1.27 cm polyethylene films, 1.25 mg/cm^2 thick, glued onto two nylon wires spaced 0.5 inches apart in the target holder. A thorium alpha source (8.78 and 6.05 MeV alphas) was positioned at the base of the target holder and the whole assembly could be moved up or down through a vacuum tight seal at the top of the scattering chamber to align either the source or targets in front of the counters.

The solid state counter was tested first. Preliminary work with C^{12} reaction alphas indicated that incomplete charge collection occurred for bias setting up to about 90 volts and a setting of 110 volts was used to remedy

*ΔE vs E spectra

this. Work with natural alphas showed that the resolution worsened by about 10% of its 70 volt value when the bias was raised to 110 volts. FWHM values of about 500 keV for reaction alpha particles were typical and were attributed largely to beam spread.

The proportional counter characteristics were checked each time the gas was changed to determine the proper operating voltage and ensure that the counter was not being operated in the region of limited proportionality. This optimum voltage was between 1300 and 1600 volts for gas pressures in the vicinity of 0.4 atmospheres. In addition, the pulse height was continuously monitored in the control room to ensure that the counter windows or ballast tank were not leaking. The counter could be operated for two or three hours with no noticeable change in pulse height from a natural alpha source.

The beam energy was variable and most runs were done at proton energies of about 40 MeV. The beam spread was usually of the order of 300 to 600 keV, and the beam current between 30 and 100 nA depending on such things as ion source age, stripping foil angle and losses in the beam pipe and collimators. The beam was focused at the scattering chamber collimators, and the beam spot at the target was about 0.25 inches by 0.50 inches.

Figure 16 shows a typical $C^{12}(p,He^4)B^9$ coincidence spectra (ΔE vs E spectra) at 60^o corresponding to an integrated charge of 40 microcoulombs collected

FIGURE 16

$C^{12}(p,He^4)B^9$ COINCIDENCE SPECTRUM*

T is the energy loss threshold level.

The contour lines correspond to constant count lines at intervals of 25 counts/channel, starting at 5 counts/channel.

* (ΔE vs E coincidence spectrum)

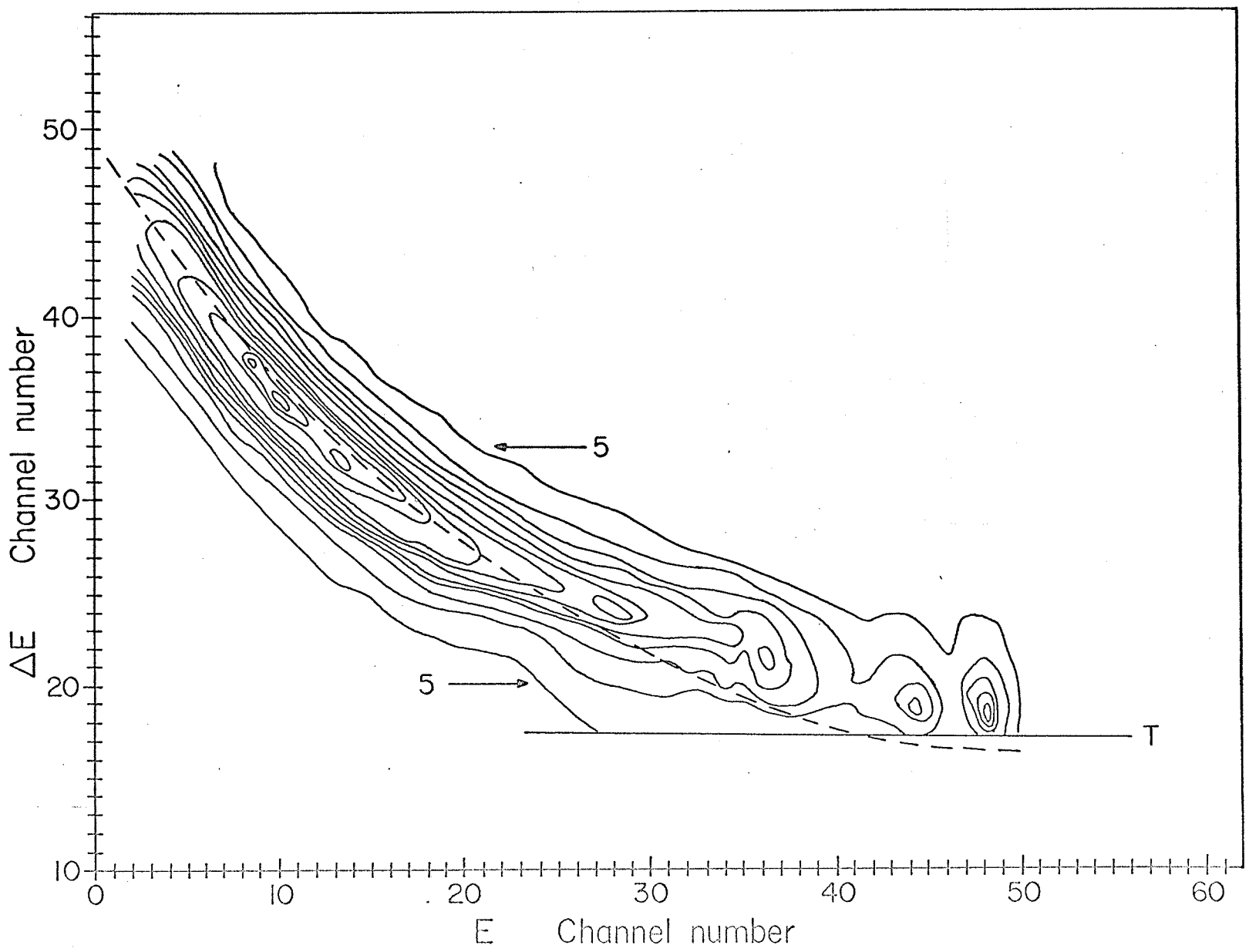
50
40
30
20
10
ΔE Channel number
5
5
T
0
10
20
30
40
50
60
E Channel number

in the Faraday cup. This reaction was considered ideal for calibration purposes since B^9 is particle unstable and decays to Be^8 by proton emission after about 10^{-19} sec. Be^8 promptly breaks up into two alpha particles and these appear as a continuum superimposed on the definite alpha energies from the first stage of the C^{12} reaction. If the energy loss is plotted against the total energy, then this continuum traces out the alpha particle hyperbola and facilitates calibration of the counter telescope system.

The continuum is shown in Figure 16 together with the alpha particles corresponding to the ground state and first two excited states of B^9 at channels 48, 44 and 36 respectively on the total energy axis. The contour lines correspond to constant count lines at intervals of 25 counts/channel starting at 5 counts/channel.

The total energy axis was calibrated by using two alpha energies from a Th source (6.05 and 8.78 MeV), taking into account the detector dead layer. For this typical example the dead layer was found to be 3.1 microns and the energy calibration yielded 470 $\pm$ 10 keV per channel.

The ΔE axis was calibrated from theoretical energy loss calculations by Aron[25] for argon gas. The incident alpha energies were calculated by working backwards from the energy lost in the solid state counter and adding the energy lost in the dead layer, proportional counter windows, and the gas. The estimated error in the initial alpha energy was estimated

to be less than 4% for energies higher than about 5 MeV.

The theoretical position of the alpha particle energy loss curve is shown by the dotted line in Figure 16. A Th source calibration yielded an energy loss of 0.83 ± 0.02 MeV at channel 34 on the energy loss axis, and this agreed with a calculated energy loss of 0.86 ± 0.07 MeV. The uncertainty in the theoretical energy loss was estimated to be about 8% and consisted primarily of the error in setting the gas pressure (about ± 5%) and in estimating the argon energy loss from Figure 2 (about ± 5%). The theoretical and experimental curves agreed within experimental error.

The resolution of the system was measured for the alphas corresponding to the ground and first excited state of B^9 and yielded FWHM values of 590 keV and 200 keV for the energy and energy loss respectively.

The incident proton energy was calculated using a program developed by Li[39] for the kinematics of the $C^{12}(p,He^4)B^9$ reaction. Figure 17 shows the theoretical relationship between beam energy and alpha particle energy at various reaction angles, for alphas corresponding to the ground state of B^9. The experimental alpha energies were corrected for energy loss in the dead layer, proportional counter and target, and yielded a proton beam energy of 39.9 ± 1.0 MeV for the run shown in Figure 16. Some preliminary work with a $C^{12}(p,He^4)B^9$ reaction at angles between 25° and 100° showed that alpha energies at various angles were accurately predicted

FIGURE 17

PROTON ENERGY vs. ALPHA ENERGY
FOR THE $C^{12}(p,He^4)B^9_{g.s.}$ REACTION

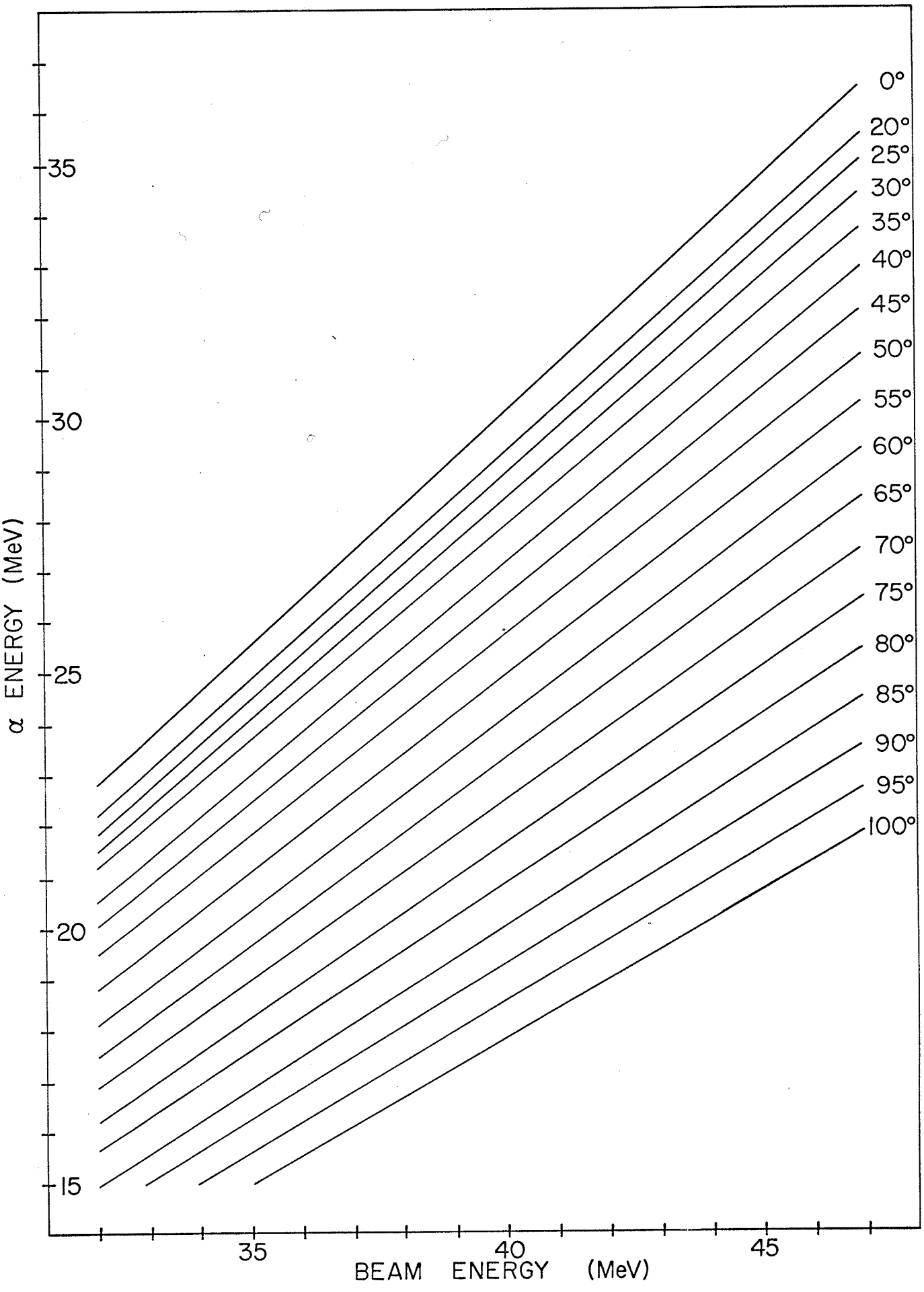
0°
20°
25°
30°
35°
40°
45°
50°
55°
60°
65°
70°
75°
80°
85°
90°
95°
100°
35
30
25
20
15
α ENERGY (MeV)
35
40
45
BEAM ENERGY (MeV)

by this kinematic method and indicated that working backwards to get at the beam energy was a valid procedure.

Figure 16 shows that the position of the alpha particle hyperbola can be predicted and this meant that the positions of the loci of other z groups could be inferred from theoretical considerations.

The system had an energy threshold of about 5 MeV for alpha particles, 7 MeV for He^6, and 11 MeV for Li^6. At energies above their respective threshold levels, the unique identification of He^6 and Li^6 should be possible, even in an alpha background. Figure 16 shows that the FWHM of the energy loss spectrum for alpha particles at a given energy is about 30% of the theoretical energy loss at 7 MeV and less at higher energies. Since the theoretical energy losses in argon for He^6 and Li^6 respectively are at least 1.3 and 2.6 times that of He^4 (above 7 MeV), then any He^4 background should not mask the counts of these heavy particles if they are of comparable intensity.

Calibration of the Electrostatic Separator

Two alpha energies corresponding to the ground and first excited state of B^9 in a $C^{12}(p,He^4)B^9$ reaction were used to calibrate the separator for higher energy particles. The technique employed was similar to that described previously pp. 53 to 55) for tests with natural alpha particles.

The number of counts at the solid state detector was recorded as the separator voltage was increased and the resulting transmission spectra were similar to the one shown in Chapter 4 for natural alpha particles (Figure 11). Both narrow and wide targets were used (0.32 cm and 1.27 cm) and two different separator radii were employed - 445 cm and 348 cm. The counter collimator had an aperture diameter of 8.4 mm.

The separator voltages at which maximum alpha transmission occurred agreed with the theoretically calculated positions within experimental error. For example the transmission voltage for 23.8 MeV alphas was found to be 41 $\pm$ 2 kV experimentally, and 43 kV theoretically (equation 4.6). In addition, there was no significant difference between the number of counts observed at the transmission peak and the number calculated geometrically, with the separator in place. The ratio of these counts was 0.9 $\pm$ 0.1 and agreed with a similar measurement for natural alpha particles (p. 55).

The resolutions of the transmission curves were about 60% for the wide target and about 40% for the narrow target. The resolutions referred to are the ratios, in percent, of FWHM values to the voltage at maximum transmission.

It was concluded that the separator substantially reduced the elastic scattered proton background. The proton beam energy was about 40 MeV and elastically scattered protons lost about 1.5 MeV in the detector. Since the total noise level was of this order, the protons were not analyzed and

no direct measure of their transmission was possible. However, deuterons from a $C^{12}(p,d)C^{11}_{g.s.}$ reaction lost about 5 MeV in the detector and at a separator voltage setting for maximum transmission of 24 MeV alphas it was found that the 17 MeV deuteron intensity was reduced to one third of its normal value.

$C^{12}(p,He^4)B^9$ Coincidence Spectra* with Particle Separation

A $C^{12}(p,He^4)B^9$ reaction was studied with both counters and the electrostatic separator. The transmission properties were identical with those discussed in the preceeding section and the shape of the energy loss versus energy coincidence curve was similar to all previous work (Figure 16). By varying the separator voltage, it was possible to display sections of this curve with FWHM values along the total energy axis equal to about 40% of the energy at maximum transmission.

* ΔE vs E spectra

CHAPTER 8 DIFFERENTIAL CROSS SECTIONS

$C^{12}(p,He^4)B^9$

Angular distributions of alpha particles from a $C^{12}(p,He^4)B^9$ reaction were taken over a range from 30^o to 90^o to check the equipment and compare the results with those of other workers. The electrostatic separator was not used. Figure 18 shows a $C^{12}(p,He^4)B^9_{g.s.}$ alpha particle angular distribution at 43.5 MeV compared to one taken by Hird et al.[40] at 45 MeV. The upper curve at 43.5 MeV has been arbitrarily normalized. Nevertheless, the two curves agree qualitatively in shape.

The target was a polyethylene foil 1.25 mg/cm^2 thick and measured 1.25 cm by 1.91 cm.

No attempt was made to determine the theoretical reaction mechanism. Hird and Li[41] have investigated this reaction in detail and concluded that the mechanism is likely triton pick-up with direct exchange stripping accounting for the backward peaking.

Li^6 Reaction Particle

The equipment was used to look for a (p,Li^6) reaction in two readily available targets (C^{12} and F^{19}) at forward angles.

These reactions were thought to be unlikely. Both could involve He^5 pickup and since neither nucleus has 2

FIGURE 18

$C^{12}(p,He^4)B^9_{g.s.}$ DIFFERENTIAL CROSS SECTION

43.5 MeV (this work)

△ 45 MeV (Hird et al[40])

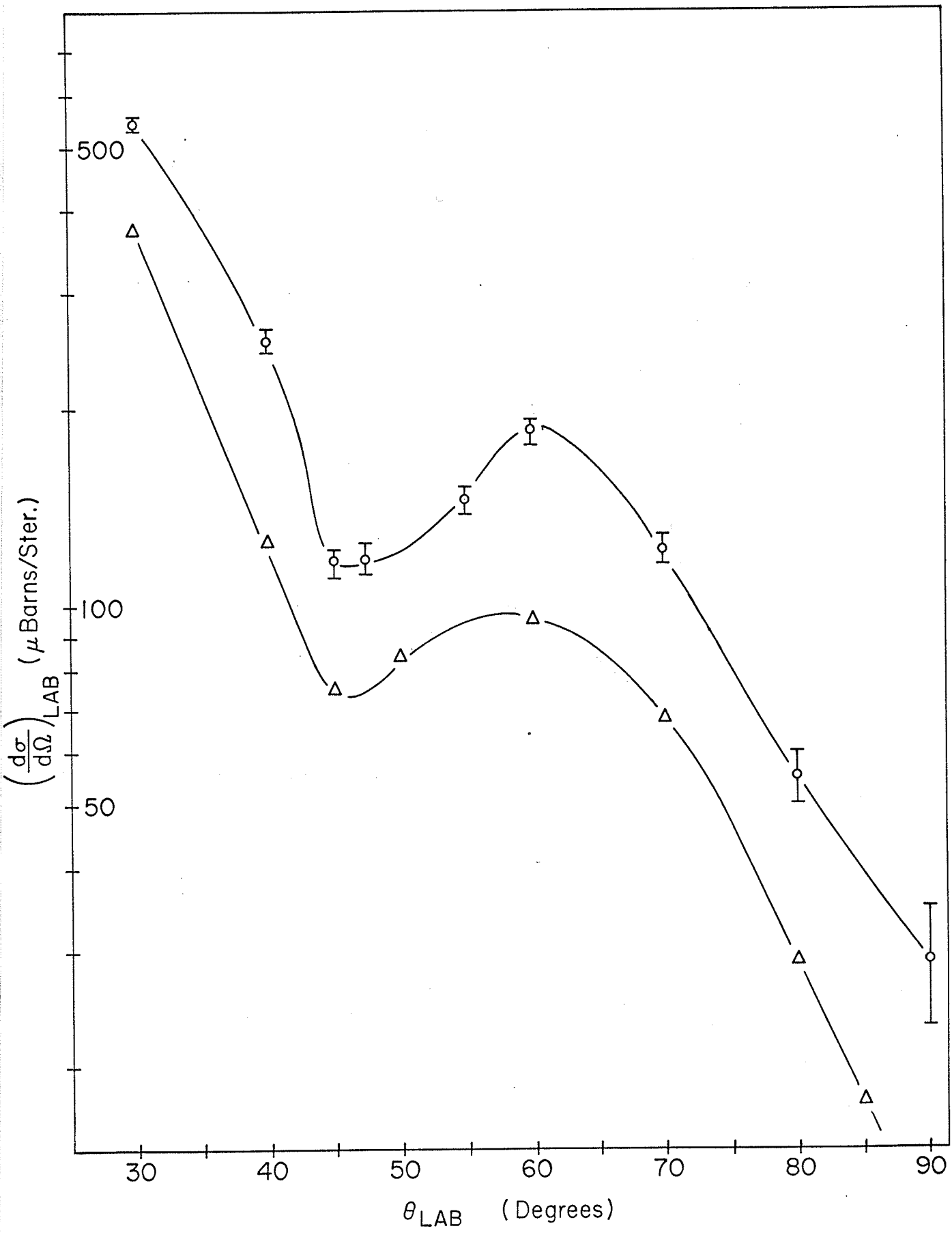
500
100
50
$\left(\frac{d\sigma}{d\Omega}\right)_{LAB}$ (μBarns/Ster.)
30
40
50
60
70
80
90
θ_{LAB} (Degrees)

protons and 3 neutrons above a closed shell this pickup is probably unlikely. Moreover, there is no theoretical reason for He^5 clustering in either nucleus since C^{12} is well described by an alpha particle model and F^{19} by an O^{16} core and a triton, and thus an exchange process is unlikely. If the Li^6 reaction does exist, it would be less probable in F^{19} since the O^{16} closed shell would have to be broken.

The targets were foils - 1.25 mg/cm^2 polyethylene and 3.14 mg/cm^2 teflon. The teflon target was changed each time 100μC were collected in the Faraday cup since the target was destroyed after about 150μC were collected.

Some kinematic calculations indicated that the ground state Li^6 group would have an energy of about 20 MeV for a $C^{12}(p,Li^6)Be^7$ reaction and about 30 MeV for $F^{19}(p,Li^6)N^{14}$ in the forward direction, corresponding to a proton beam energy of about 45 MeV.

Alpha particles from a $C^{12}(p,He^4)B^9$ reaction were used to calibrate the equipment as described in Chapter 7 and the energy loss gain lowered so that the Li^6 hyperbola would be displayed on the 64 x 64 grid of the pulse height analyzer. The electronic systems were checked and found to be linear and free from saturation effects.

A search for the $F^{19}(p,Li^6)N^{14}$ reaction at two angles in the forward direction (20° and 25°) yielded negative results.

At 25°, the equipment was checked with alpha particles from a $C^{12}(p,He^4)B^9$ reaction to ensure that the apparatus was functioning properly. The proportional counter gain was then dropped and the energy loss axis calibrated with 8.78 MeV alphas from Po^{212}. Figure 19 shows the coincidence spectrum after 175 μC were collected in the Faraday cup at a proton beam current of about 70 nA. Energy calibrations yielded 640 ± 13 keV/channel and 62 ± 5 keV/channel along the energy and energy loss axes respectively. The constant counts/channel contour lines just above the threshold level correspond to alpha particles of low energy. There were no counts whatsoever near the calculated Li^6 hyperbola and only a few counts (less than 4 counts/channel) beyond the contour line corresponding to 5 counts/channel.

After examination of various coincidence spectra, it was concluded that a peak could be identified in a region of low (less than 5 counts/channel) background if about 10 or 20 counts were contained under the peak. Since no counts were observed near the calculated position of the Li^6 hyperbola, it was concluded that the probability for the $F^{19}(p,Li^6)N^{14}$ reaction was low at proton energies of about 40 to 50 MeV.

The counts under the ground state alpha peak of the $C^{12}(p,He^4)B^9$ reaction shown in Figure 16 was about 1100 - corresponding to an accumulated charge of 40 μC in the Faraday cup. The differential cross section at this angle (60°) was about 100 μb/sr (Figure 18). This information was used to

FIGURE 19

COINCIDENCE SPECTRUM* FROM F^{19} TARGET

T is the energy loss threshold level.

The curve marked Li^6 is the theoretical position of Li^6 reaction particles.

The numbers in the lower left hand corner label the number of counts/channel for each contour line.

* (ΔE vs E coincidence spectrum)

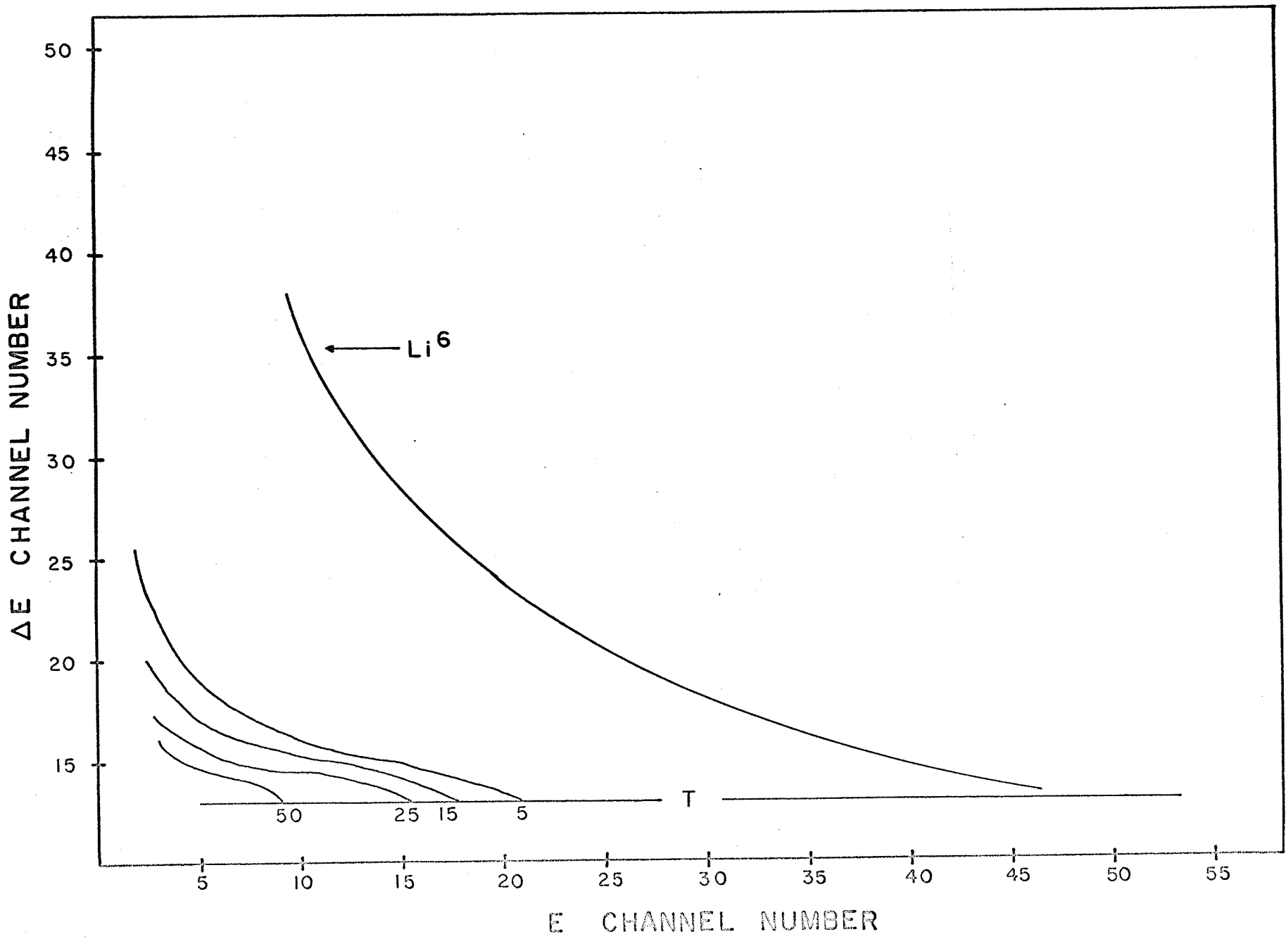
ΔE CHANNEL NUMBER
50
45
40
35
30
25
20
15
Li6
T
50
25
15
5
5
10
15
20
25
30
35
40
45
50
55
E CHANNEL NUMBER

estimate the differential cross section for a reaction leading to 25 counts under a peak in a coincidence spectrum, and an accumulated charge of 175 μC, and yielded $d\sigma/d\Omega \sim 0.5$ μb/sr.

The differential cross section of the $F^{19}(p,Li^6)N^{14}$ reaction was thus estimated to be not more than 0.5 μb/sr.

The experiment was repeated at 25°, with increased proportional counter gain, to examine the higher energy region of the coincidence spectrum. An energy calibration yielded 28 $\pm$ 2 keV/channel along the energy loss axis and 640 $\pm$ 13 keV/channel on the energy axis. No Li^6 particles were detected. A similar experiment at 20° yielded the same negative results. 300 μC were collected at a beam current of about 60 nA.

A search for Li^6 from a C^{12} target was also unsuccessful. Experiments were performed at angles of 60°, 35°, and 25° in the forward direction, with 80 μC, 180 μC, and 200 μC collected at the Faraday cup respectively. The experimental techniques employed were similar to the F^{19} method discussed above, and the coincidence spectra were similar to Figure 19. No Li^6 peaks were detected in the spectra and the maximum differential cross section for the (p,Li^6) reaction in C^{12} was also estimated to be about 0.5 μb/sr.

REFERENCES

1 A.E. Glassgold & A. Galonsky, Phys.Rev. 103, 701, (1956)

2 G.C. Phillips & T.A. Tombrello, Nuc.Phys. 19, 555, (1960)

3 W.W. Daehnick & L.J. Denes, Phys.Rev. B136, 1325, (1964)

4 D.S. Gemmel, J.R. Erskine, & J.P. Schiffer, Phys.Rev. B134, 710, (1964)

5 D. Dehnhard, D.S. Gemmel, & Z. Vager, Bull.Am.Phys.Soc. 10, 462, (1965)

6 F.W. Slee, Bull.Am.Phys.Soc. 10, 461, (1965)

7 R.H. Lindsay, Phys.Rev. 147, 792, (1966)

8 M. Furukawa, S. Kume, M. Ogawa, Nuc.Phys. 69, 362, (1965)

9 D.W. Heikkinen, Phys.Rev. 141, 1007, (1966)

10 H.A. Bethe & J. Ashkin, "Passage of Radiations through Matter" in Experimental Nuclear Physics, edited by Segrè, Vol.I, p.166 (John Wiley & Sons, 1953)

11 C. Williamson & J.P. Boujot, Tables of Range and Rate of Energy Loss of Charged Particles of Energy 0.5 to 150 MeV, Centre D'Etudes Nucléaires De Saclay (CEA) Report no. 2189, (1962)

12 D.H. Wilkinson, Ionization Chambers and Counters, (Cambridge University Press, 1950)

13 B.B. Rossi & H.H. Staub, Ionization Chambers and Counters, (McGraw-Hill, 1949)

14 W. Franzen & L.W. Cochran, "Pulse Ionization Chambers and Proportional Counters" in Nuclear Instruments and their Uses, edited by Snell, Vol.I (John Wiley & Sons, 1962)

15 L.H. Gray, Proc. Cambridge Phil.Soc. 40, 72, (1944)

16 W.P. Jesse, H. Forstat, & J. Sadauskis, Phys.Rev. 77, 782, (1950)

17 T.E. Bortner, G.S. Hurst, & W.G. Stone, Rev.Sci.Instr. 28, 103, (1957)

18 L.D. Landau, J.Phys. U.S.S.R. 8, 201, (1944)

19 K.R. Symon, Ph.D. Thesis, (Harvard University, 1948)

20 S.M. Seltzer & M.J. Berger, "Energy Loss Straggling of Protons and Mesons" in Studies in Penetration of Charged Particles in Matter, p. 187, National Academy of Sciences - National Research Council, Washington, D.C., Pub. 1133 (1964)

21 B.B. Rossi, High Energy Particles, (Prentice-Hall, 1952)

22 P.V. Vavilov, JETP 5, 749, (1957)

23 U. Fano, Phys. Rev. 72, 26, (1947)

24 H.S. Snyder, Phys.Rev. 72, 181, (1947)

25 W.A. Aron, B.G. Hoffman, & F.C. Williams, U.S.A.E.C. Report AECU-663, (1951)

26 W.W. Daehnick & L.J. Denes, University of Pittsburgh, private communication, (1965)

27 B. Cork, "Beam Separators" in Methods of Experimental Physics, edited by Yuan and Wu, Vol.5, Pt.B, p. 747, (Academic Press, 1963)

28 C.A. Ramm, Proc.Int.Conf. on Instrumentation for High Energy Physics, Lawrence Radiation Laboratory, p. 289 (Interscience Publishers, 1960)

29 O. Chamberlain, Ann.Rev. of Nuc.Sci. 10, 161, (1960) and references therein

30 K.T. Bainbridge, "Charged Particle Dynamics and Optics", in Experimental Nuclear Physics, edited by Segre, Vol.1, p. 592, (John Wiley & Sons, 1953)

31 J.J. Murray, p. 25 in reference 28

32 F. Rohrbach, CERN Report 64-50, (1964)

33 R.N. Stokes, J.A. Northrop, & K. Boyer, Rev.Sci.Instr. 29, 61, (1958)

34 D.A. Bromley, M.W. Sacks, & C.E. Anderson, Proc. of Symp. on Nuc.Instr., Harwell, edited by Birks, p. 67, (1962)

35 C.D. Goodman & J.B. Ball, p. 163 in reference 34

36 F. Goulding, Nuc. Inst. and Methods 31, 1, (1964)

37 S.K. Mark, University of Manitoba, private communication, (1966)

38 K.G. Standing & J.J. Burgerjon, IEEE Trans., Nuc. Sci. NS 13, No 4, 422, (1966)

39 T.Y. Li, University of Manitoba, private communication, (1965)

40 B. Hird, T.Y. Li & C.J. Kost, University of Manitoba, private communication, (1966)

41 R.M. Craig, B. Hird, C.J. Kost & T.Y. Li, "The (p,α) Reaction Mechanism at 45 MeV", Physics Letters 21, 177, (1966)